

NASA/TM-2010-216209



# Landing Gear Components Noise Study – PIV and Hot-Wire Measurements

*Florence V. Hutcheson and Casey L. Burley  
Langley Research Center, Hampton, Virginia*

*Daniel J. Stead and Lawrence E. Becker  
Lockheed Martin Engineering and Sciences, Hampton, Virginia*

*Jennifer L. Price  
National Institute of Aerospace, Hampton, Virginia*

## NASA STI Program . . . in Profile

Since its founding, NASA has been dedicated to the advancement of aeronautics and space science. The NASA scientific and technical information (STI) program plays a key part in helping NASA maintain this important role.

The NASA STI program operates under the auspices of the Agency Chief Information Officer. It collects, organizes, provides for archiving, and disseminates NASA's STI. The NASA STI program provides access to the NASA Aeronautics and Space Database and its public interface, the NASA Technical Report Server, thus providing one of the largest collections of aeronautical and space science STI in the world. Results are published in both non-NASA channels and by NASA in the NASA STI Report Series, which includes the following report types:

- **TECHNICAL PUBLICATION.** Reports of completed research or a major significant phase of research that present the results of NASA programs and include extensive data or theoretical analysis. Includes compilations of significant scientific and technical data and information deemed to be of continuing reference value. NASA counterpart of peer-reviewed formal professional papers, but having less stringent limitations on manuscript length and extent of graphic presentations.
- **TECHNICAL MEMORANDUM.** Scientific and technical findings that are preliminary or of specialized interest, e.g., quick release reports, working papers, and bibliographies that contain minimal annotation. Does not contain extensive analysis.
- **CONTRACTOR REPORT.** Scientific and technical findings by NASA-sponsored contractors and grantees.

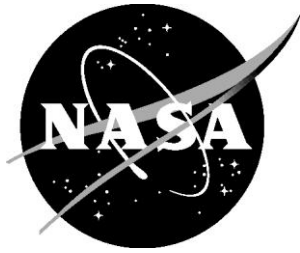
- **CONFERENCE PUBLICATION.** Collected papers from scientific and technical conferences, symposia, seminars, or other meetings sponsored or co-sponsored by NASA.
- **SPECIAL PUBLICATION.** Scientific, technical, or historical information from NASA programs, projects, and missions, often concerned with subjects having substantial public interest.
- **TECHNICAL TRANSLATION.** English-language translations of foreign scientific and technical material pertinent to NASA's mission.

Specialized services also include creating custom thesauri, building customized databases, and organizing and publishing research results.

For more information about the NASA STI program, see the following:

- Access the NASA STI program home page at <http://www.sti.nasa.gov>
- E-mail your question via the Internet to [help@sti.nasa.gov](mailto:help@sti.nasa.gov)
- Fax your question to the NASA STI Help Desk at 443-757-5803
- Phone the NASA STI Help Desk at 443-757-5802
- Write to:  
NASA STI Help Desk  
NASA Center for AeroSpace Information  
7115 Standard Drive  
Hanover, MD 21076-1320

NASA/TM-2010-216209



# Landing Gear Components Noise Study – PIV and Hot-Wire Measurements

*Florence V. Hutcheson and Casey L. Burley  
Langley Research Center, Hampton, Virginia*

*Daniel J. Stead and Lawrence E. Becker  
Lockheed Martin Engineering and Sciences, Hampton, Virginia*

*Jennifer L. Price  
National Institute of Aerospace, Hampton, Virginia*

National Aeronautics and  
Space Administration

Langley Research Center  
Hampton, Virginia 23681-2199

March 2010

Available from:

NASA Center for Aerospace Information (CASI)  
7121 Standard Drive  
Hanover, MD 21076-1320  
443-757-5802

**Landing Gear Components Noise Study –  
PIV and Hot-Wire Measurements**

Florence V. Hutcheson and Casey L. Burley  
*Aeroacoustics Branch/RTD*

Daniel J. Stead and Lawrence E. Becker  
*Lockheed Martin Engineering and Sciences*

Jennifer L. price  
*National Institute of Aerospace*

*NASA Langley Research Center  
Hampton, VA 23681*

**Abstract**

PIV and hot-wire measurements of the wake flow from rods and bars are presented. The test models include rods of different diameters and cross sections and a rod juxtaposed with a plate. The latter is representative of the latch door that is attached to an aircraft landing gear when the gear is deployed, while the single and multiple rod configurations tested are representative of some of the various struts and cables arrangements present on an aircraft landing gear. The test set-up is described and the flow measurements are presented. The effect of model surface treatment and freestream turbulence on the spanwise coherence of the vortex shedding is studied for several rod and bar configurations.

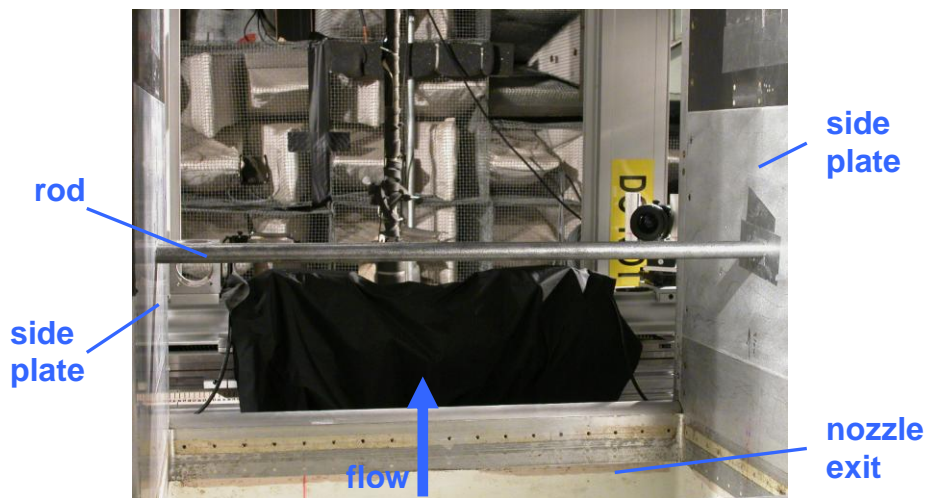
## 1. Introduction

During airport approach, the noise radiated from aircraft landing gears is a dominant airframe noise source. A number of numerical<sup>1-7</sup> and experimental studies<sup>8-10</sup> have been conducted in order to identify and model the noise generation mechanisms of landing gear configurations. Noise reduction studies<sup>11</sup> are also ongoing. Since many components of a landing gear (the struts, the cables, the axles) can be modeled by rods of various lengths and cross-sections, understanding the generation mechanisms of the noise radiated from single and multiple rod configurations is of relevance to the landing gear noise reduction effort.

In the present study, PIV, hot-wire and acoustic measurements were obtained for single and two rod configurations to investigate the effect of incoming turbulence, yaw angle, proximity and wake interference on the rod's vortex shedding and on the radiated noise. The PIV measurements will be used in a subsequent study to characterize the turbulence in the wake of the rod elements. This information, along with the hot-wire data, will be used to develop improved flow and noise prediction models. The acquisition of the PIV and hot-wire measurements is described in this paper and the results obtained are presented. Results from the acoustic study are presented in ref. 12.

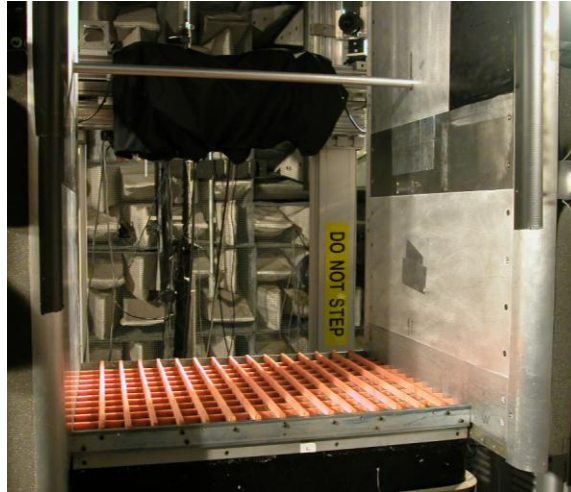
## 2. Test description

The PIV and hot-wire measurements for this landing gear noise component experiment were performed at NASA Langley Research Center in the Quiet Flow Facility (QFF). The QFF is an open jet facility equipped with a 2 by 3 foot rectangular open jet nozzle. The rods were supported 19" above the nozzle by two vertical side plates that are mounted to the short sides of the nozzle (see Figure 1).



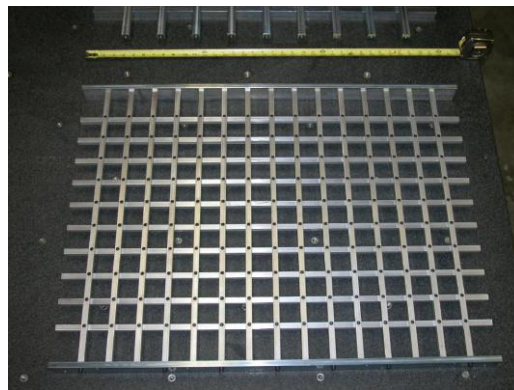
**Figure 1.** Test set-up

For some of the rod configurations tested, a turbulence generating grid was mounted across the exit plane of the nozzle (as shown in Figure 2). The purpose of the grid was to generate known turbulence upstream of the rods for study of rod configurations in clean and freestream turbulent flow. Acoustic foam treatment was glued along each bar of the turbulence grid to attenuate noise from the air flowing through the grid. When a turbulence grid was used, the rods were mounted 40" downstream of the nozzle exit plan, in a region of the flow where the generated turbulence is assumed to be homogeneous based on the grid geometry<sup>13</sup>.



**Figure 2.** Turbulence grid with acoustic foam mounted on the nozzle.

The turbulence grid, shown in Figure 3, was designed such that it would generate macro-scales (integral scale) ranging between 0.5" to 0.92" and micro-scales (dissipation scale) ranging between 0.07" to 0.12". The grid bars were 0.5"x 0.5" in cross section, and the spacing (center to center) between consecutive bars was 2.22".



**Figure 3.** Grid for generation of small scale turbulence.


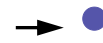


## 2.1 Model configurations

Square and circular aluminum rods of 3 ft length were tested. Measurements were taken at flow mach numbers of 0.13 and 0.17 (when the turbulence grid was used, measurements were taken only at 0.13 Mach number). PIV and hot-wire measurements were taken in the wake of single and multiple rods configurations. These configurations are listed below in Table 1. Measurements were taken for both smooth and gritted model surfaces (#90 grit was used for the gritted configurations). Hot-wire measurements were taken for only a subset of the configurations listed in Table 1, namely configurations 1, 2, 9, 13, 20 and 21.




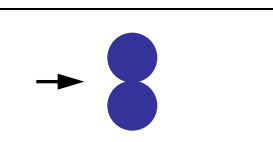
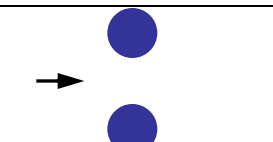

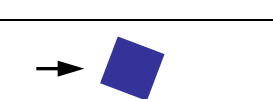
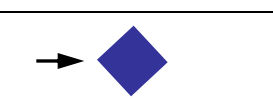
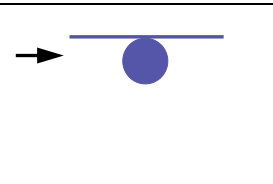
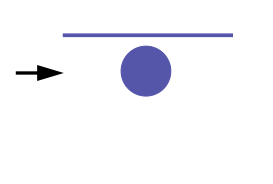
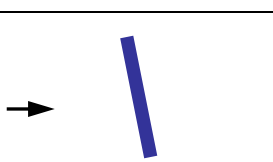
Several concepts for the reduction of the noise radiating from a cylindrical rod were examined. These concepts were inspired by an experiment conducted by Ahuja et al.<sup>14</sup> to reduce the noise radiating from car antennas. In that experiment, protrusions in the form of O-rings and beads were distributed along the span of a conical rod immersed in a uniform flow. It was shown that the protrusions reduced the radiated noise by rendering the vortex shedding along the span of the rod less coherent. It is also mentioned in ref.14 that similar results can be achieved by wrapping a wire along the span of the rod.



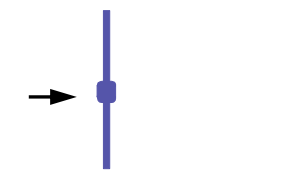

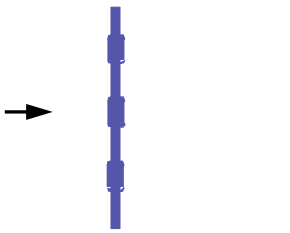
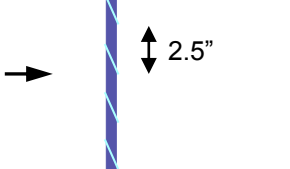
In the present study, the effect of collars (configuration 20) and wire wraps (configuration 21) on the noise radiated by a cylindrical rod was examined. The collars are uniformly distributed along the span of the rod and the wires are wrapped along the entire span of the rod. Hot-wire measurements were performed to determine the effect of the collars and wire wraps on the vortex shedding spanwise coherence. Preliminary microphone measurements were also acquired to obtain an initial measure of the impact of the collars and wire wraps on the radiated noise level.

**Table 1.** Model configurations.

Configuration	Sketch (cross-sections)	Description
1		1" diameter rod
2		1/2" diameter rod
3		Two 1" diameter rods together.
4		Two 1" diameter rods, centers 2" apart.



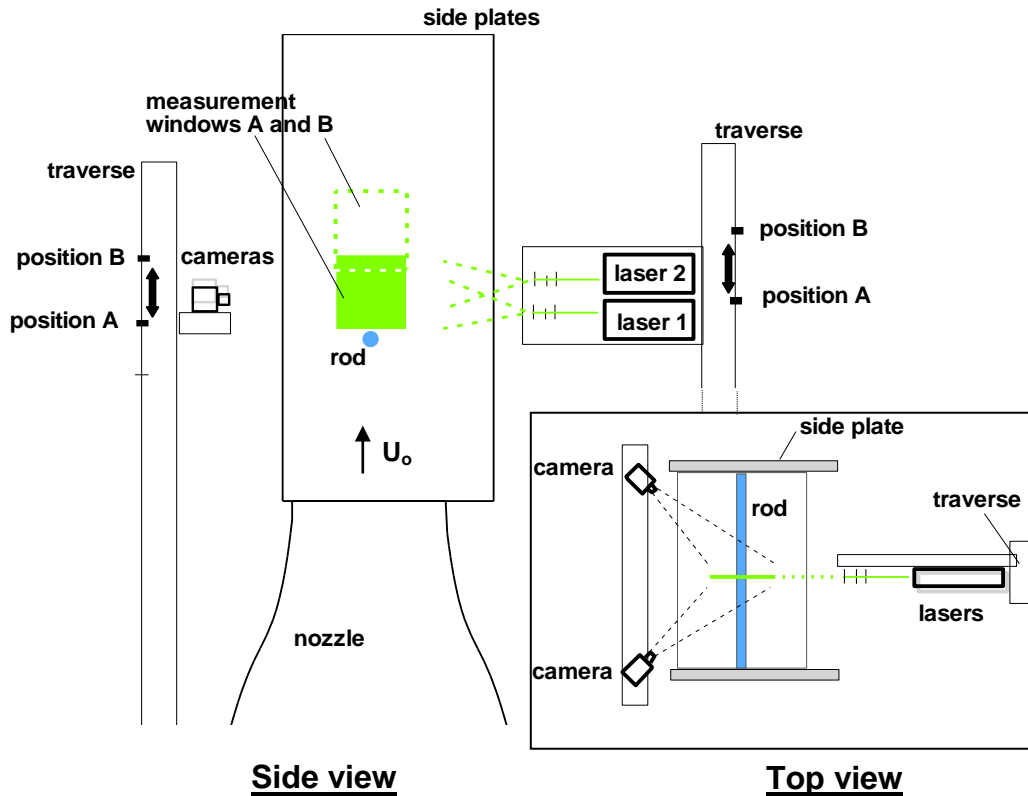
5		Two 1" diameter rods, centers 3" apart.
6		1" diameter rod upstream of a 1/2" rod, centers 3" apart.
7		1/2" diameter rod upstream of a 1" rod, centers 3" apart.
8		Two 1" diameter rods, centers 1" apart and aligned perpendicular to flow.
9		Two 1" diameter rods, centers 2" apart and aligned perpendicular to flow.
10		Square bar (1"x1" cross section) with two sides parallel to flow.
11		Square bar (1"x1" cross section) with 2 sides at 30° with flow .
12		Square bar (1"x1" cross section) with 2 sides at 45° with flow.
13		3/4" diameter rod with 4" wide by 0.2" thick plate (same span as rod), no gap. Rod secured to plate with 17 evenly spaced brackets. The edges of the plate are beveled down to 0.04" over a distance of 0.27".
14		3/4" diameter rod with 4" wide by 0.2" thick plate (same span as rod), 0.1" gap. Rod secured to plate with 17 evenly spaced brackets. The edges of the plate are beveled down to 0.04" over a distance of 0.27".
Configuration	Sketch (spanwise views)	Description
15		1" diameter rod, axis 15° from plane perpendicular to flow.

16		1" diameter rod, axis 30° from plane perpendicular to flow.
17		1" diameter rod perpendicular to flow and 1/2" diameter rod with axis 30° from 1" rod axis. Distance between rod centers at mid span is 3".
18		1/2" diameter rod perpendicular to flow with a 1"x1" cylindrical collar (with rounded edges) located at mid-span.
19		1/2" diameter rod perpendicular to flow with a 1"x1" square collar located at mid-span.
20		1/2" diameter rod perpendicular to flow with eleven collars (1.5" long, 3/4" in diameter, rounded edges) centered every 3.1".
21		1/2" diameter rod perpendicular to flow with 1/8" wire wrapped along the full span of the rod.

## 2.2 PIV system set up

The PIV system set up is described in Figure 4. As shown in this figure, flow field measurements were performed downstream of the rod elements using stereo PIV. Such PIV configurations yield three components (3-C) of velocity over a two-dimensional plane. The PIV measurements were obtained for two PIV window locations downstream of the models. For most of the configurations, the measurements were taken at the model mid-span and in a plane parallel to the test section walls (i.e., parallel to the side plates). The first measurement location, window A, was located directly above the rod (or directly above the most downstream rod for multiple rods configurations). The distance between the bottom edge of the measurement location and the rod surface was

approximately 1mm. Window A covered a 10” by 10” area. A second measurement location, window B, was located 8.5” further downstream. Window B covered also a 10” by 10” area which overlapped the first measurement area defined as window A by approximately 1.5”.



**Figure 4.** Illustration of PIV system set-up (not to scale).

The PIV measurement planes were illuminated using two Nd:YAG, 120 mJ, double cavity lasers with a repetition rate of 15 Hz. To minimize laser reflections from the test model, beam-blocks were used to “chop off” the light sheet as close as possible to the model surface. The thickness of the light sheet was about 1 mm.

Two Redlake MegaPlus ES 1.0 CCD cameras with 105 mm lenses were used to record the PIV images with a resolution of 1008 by 1012 pixels. The lasers, optical lenses and cameras were mounted on a traverse system in order to maintain the distance between the cameras and the light sheet constant while moving to the different measurement locations.

The flow was seeded upstream of the low-pressure air fan (i.e., at the beginning of the flow circuit) to ensure a homogeneous distribution of the seeded particles throughout the

jet flow. Laskin nozzle seeders filled with Bis(2-Ethylhexyl) Sebacate were used to generate particles of less than 1  $\mu\text{m}$  in diameter.

Over 400 image pairs were acquired at each measurement location, at a rate of 15 frames per second (the frame rate was synchronized with that of the laser pulse). Integrated Design Tools proVISION software (version 2.01.08) was used to process the PIV images and generate 3-component velocity vector maps. The PIV images were processed with a 24 by 24 interrogation window size with a 50% overlap, leading to a resolution of 1 velocity vector for each 1.15 mm by 0.94 mm area. Cross-correlation techniques<sup>18</sup> were used to compute the velocity vectors from PIV image pairs. The percentage of interpolated velocity vectors computed in each vector map was kept below 1% (an interpolated vector is the result of a least square interpolation of nearest neighbors).

### 2.3 Hot-wire system set up

The hot-wire measurements were acquired using two straight hot-wire probes. Platinum-plated tungsten wires with a diameter of 5  $\mu\text{m}$  and unplated active length of 0.13 cm were used. The resistance of the wires ranged between 3.4 and 3.8 Ohms. An overheat ratio of 1.8 was used. The wires were operated using a TSI IFA 100 constant temperature anemometer (CTA) and were tuned for a frequency response of approximately 80 kHz. The bridge output of the CTA was obtained in NetCDF format using a NEFF system 495 data acquisition unit using a 12-bit A/D converter. The data was sampled at a rate of 142.8 kHz. The signal was separated into AC and DC components to maximize the available system gain. At each measurement location, 2,048,000 data points were taken yielding just over 14 seconds worth of data.

A five-hole pitot-static tube was used in conjunction with the hot-wire probes in order to verify the hot-wire measurements. The pressure measurements were obtained with a PSI system 8400 data acquisition unit which was accurate within  $\pm 0.0025$  psi. The hot-wires were calibrated frequently throughout the duration of the test. These calibrations were performed measuring both flow velocity and wire voltages. A 4<sup>th</sup> order polynomial fit was applied to the data to obtain calibration curves.

The hot-wire measurements were acquired with one wire remaining stationary at the model mid-span while the second hot-wire traversed the flow in increments in either the spanwise (x) or cross-stream (z) direction (see Figure 5 and 6). Cross-stream surveys were performed for configurations 1, 9 and 13 at the following downstream locations:  $x_1 \cong 0.5''$  (i.e., as close as possible to the rod surface),  $x_2 = 1.5''$  and  $x_3 = 5.5''$ , where  $(x,y,z) = (0,0,0)$  is on the axis of the rod at the model mid-span. For each of the aforementioned  $x_i$ ,  $i=1,2,3$  locations, the stationary wire was located at  $(x_i, 0, 0)$  while the traversing wire was moved from  $(x_i, 0, -2'')$  to  $(x_i, 0, +2'')$  with an increment  $\Delta z$  of 0.5'' between each measurement location. For configuration 9, in which a second rod is placed parallel to the first one at  $z = -2''$ , the cross-stream survey extended between  $z = -4''$  and  $z = 2''$  with  $\Delta z = 0.5''$ . For configuration 13, because of the plate that is attached to the rod, the cross-stream survey at  $x \cong 0.5''$  extended only between  $z = 0$  and  $z = 2''$ .

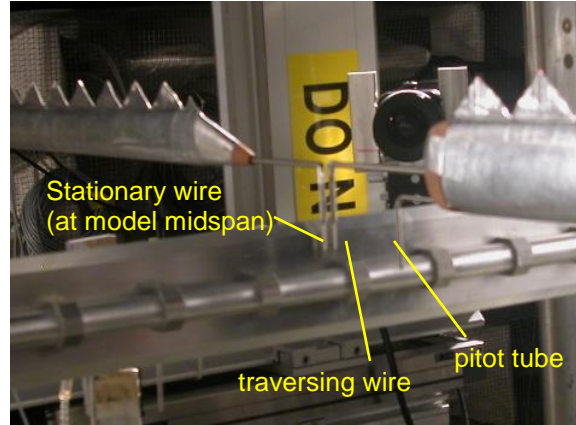


Figure 5. Hot-wire probes set-up.

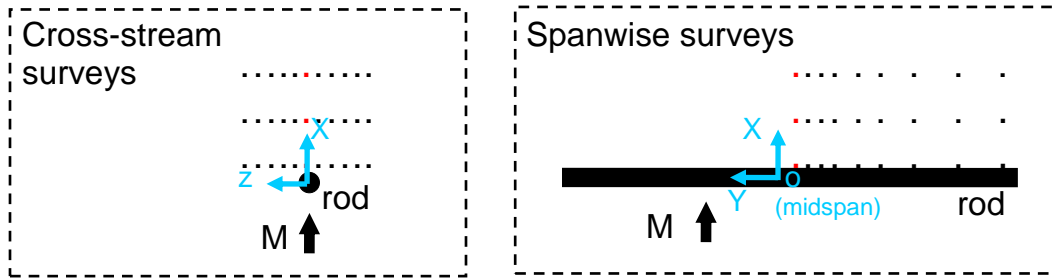


Figure 6. Hot-wire cross-stream and spanwise surveys.

Spanwise surveys were performed for configurations 2, 20 and 21 at downstream locations  $x_4=0.5''$ ,  $x_5=0.75''$  and  $x_2=1.5''$ . For configurations 1, 9 and 13 a spanwise survey was performed only at downstream location  $x_1=0.5''$ . For each of the aforementioned  $x_i$ ,  $i=1$  or  $2,4,5$  locations, the stationary wire was located at  $(x_i,0,0)$  while the traversing wire was moved to each of the following spanwise locations:  $(x_i,y,0)$  where  $y=0.25''$ ,  $0.5''$ ,  $0.75''$ ,  $1''$ ,  $y=1''+0.5''k$  ( $k=1,2,\dots,8$ ),  $y=5''+n$  ( $n=1,2,\dots,5$ ) and  $y=13''$  and  $17''$ .

### 3. Test results

#### 3.1. PIV results

The flow field images obtained from the PIV measurements are presented in figures 7 through 27. The results displayed were obtained with the standard data processing methodology described in section 2.3. Figures displaying the instantaneous in-plane velocity field  $(u\hat{x}+v\hat{y})$  (with the free stream velocity subtracted) and the instantaneous

axial vorticity field ( $\Omega_z = dv/dx - du/dy$ ) are shown for all the model configurations tested. For presentation clarity, the vectors in each map are only shown for every second node in x and y.

In each plot, the PIV results obtained from measurement windows A and B (see Figure 5) are shown. The plots from measurement window A show the wake flow up to 250 mm downstream of the model while the second plot shows the wake flow in the region located between 200 mm and 450 mm downstream of the model. The two plots are purposely not shown overlapped as the measurements were taken at different instants in time.

In a follow up study, various spectral decomposition techniques such as POD will be applied to these PIV measurements to characterize and define the turbulence shed by the different rod configurations tested in this experiment. This information will be used to model the turbulence shedding from landing gear components.

### 3.2. Hot-wire results

The wake flow velocity data obtained from the streamwise and spanwise hot-wire surveys were acquired to support related CFD model development. In this section only results drawn from the spanwise survey data are presented. The spanwise surveys were performed to examine the effect of incoming turbulence, surface treatment and noise reduction devices (collars and wire wrap) on the vortex shedding spanwise coherence. These results will subsequently be tied to the acoustic study since the vortex shedding spanwise coherence is related to the amplitude of the radiated noise<sup>12</sup>.

Cross spectra between the stationary and the traversing hot-wire signals were generated with a frequency resolution  $\Delta f$  of 17.4 Hz. These cross-spectra were calculated when the stationary and traversing hot-wires were located 0.25" apart (along the model span) at downstream location  $x_1$  (for model configurations 2, 20 and 21) or  $x_4$  (for model configurations 1, 9 and 13). Each cross spectrum generally displayed a small correlation peak at the frequency  $f = f_0$  and a stronger correlation peak at  $f = 2 f_0$ , where  $f_0$  corresponds to the rod vortex shedding frequency. The cross spectra obtained for the 1" rod (i.e., configuration 1) are presented in Figure 28.

The spanwise variation of the coherence  $\sqrt{\gamma^2}$  of the vortex shedding was calculated over a 5-bin frequency band centered at  $f = 2 f_0$ . The coherence is defined as

$$\gamma^2(f) = \frac{G_{ab}^2(f)}{G_{aa}(f) G_{bb}(f)} \quad (1)$$

where  $G_{ab}(f)$ ,  $G_{aa}(f)$  and  $G_{bb}(f)$  are the cross spectra and auto spectra of the stationary and traversing hot-wire signals.

The spanwise coherence for the smooth and gritted 1" rod, with and without freestream turbulence is displayed in Figure 29. The flow Mach number is 0.13. It is seen that for the smooth rod in clean flow some coherence in the vortex shedding is maintained over a span of approximately 3.5D (where D is the rod diameter). When the surface of the rod is gritted, the coherence length increases to approximately 6D. When

freestream turbulence is introduced (by the turbulence grid) and the surface of the rod is smooth, the level of spanwise coherence in the vortex shedding is seen to become very low. Once the surface of the rod is gritted, the spanwise coherence level recovers and is close to that for the clean flow test cases.

At a Mach number of 0.13, the Reynolds number for this 1” rod configuration is 77,000 (and 100,000 at Mach number 0.17). For this Reynolds number (and when the rod surface is smooth), the burst to turbulence occurs in the free shear layers near the side of the cylinder and the formation of alternate eddies takes place close to the rear of the cylinder<sup>15</sup>. It has been reported in several experimental studies<sup>16,17</sup> that in this flow regime, free stream turbulence will affect the flow past the cylinder when the integral scale  $T_s$  of the turbulence is less than the rod diameter  $D$  and a reduction of the vortex shedding coherence length will result. It was observed in these studies that for  $T_s/D < 1$ , a flow regime that would otherwise occur for higher Reynolds numbers, namely  $(100k-200k) < Re < (300k-340k)$ , was triggered. In this new flow regime, transition to turbulence occurs in the free shear layers along the separation lines. This state of flow is associated with a drop in the vortex shedding coherence length (and drop in the drag coefficient) as the three-dimensionality of the onset of the transition to turbulence affects the spanwise “uniformity” of the flow. In the present study,  $T_s/D$  is less than 1, therefore, the reduction in coherence length that was observed for the smooth rod is consistent with previous published findings<sup>16,17</sup>.

As mentioned previously, for the present test case, the vortex shedding coherence length was found to be high when the rod surface was gritted, regardless of the presence of freestream turbulence. This behavior is also consistent with a study by Batham<sup>18</sup> who suggests that the roughness turbulence triggers transition around the separation line more evenly and in doing so, the separation line is straightened, leading to higher spanwise coherence levels.

Finally, regarding the hot-wire measurements that were performed on the 1” rod configuration, it is shown in Figures 30 and 31 that the spanwise coherence scales well with the Strouhal number.

The cross spectra obtained for configuration 9 are shown in Figure 32 (for this side by side rod configuration, the two hot-wires were aligned along the span and in the center plane ( $z=0$ ) of one of the two rods). It is seen that the cross spectra again display two correlation peaks, one at the vortex shedding frequency  $f = f_0$  and the other at  $f = 2 f_0$ . The correlation peak recorded at  $f = f_0$  is stronger than for the single rod case. This could be explained by the presence of a bias gap flow between the two rods. Thus, for this side by side arrangement, narrow and wide wakes often form behind the two cylinders. The gap flow is then biased towards the narrow wake and is bistable, switching to either side, leading to an interchange of the narrow and wide near-wake behind the cylinders<sup>18</sup>. This leads to the presence of a stronger cross-stream velocity component (than in the single rod case) that the hot-wires are more able to detect, allowing a distinction between the vortices that are shed from either side of the rod. This leads to a stronger spectral peak at the vortex shedding frequency. The correlation peaks observed in the cross spectra are also broader in frequency than in the single rod case. This can probably be explained by the continuous change between narrow and wide wakes which may cause the vortex shedding frequency to drift between a higher value for the narrow wake flow and a lower value for the wider wake flow.

The spanwise coherence for the side by side rod configuration is displayed in Figure 33. The flow Mach number is 0.13. The effects of freestream turbulence and of surface roughness are found to be similar to that observed for the single rod case. The spanwise coherence is high for the gritted rods with or without freestream turbulence, and for the smooth rods in clean flow. The spanwise coherence drops when freestream turbulence is introduced and the surface of the rods is smooth. Also, as for the single rod configuration, the vortex shedding spanwise coherence for the side by side rods is found to scale well with the Strouhal number (see figures 34 and 35).

The spanwise coherence for the smooth and gritted 1/2" rod, with and without freestream turbulence is displayed in Figure 36. Results are shown for a flow Mach number of 0.13 for the freestream turbulence cases and for Mach numbers 0.13 and 0.17 for the clean flow cases. It is seen that for the clean flow cases, some coherence in the vortex shedding is maintained over a span of approximately 5D (where D is the rod diameter) when the flow Mach number is 0.13 and 6D when the flow Mach number is 0.17. It is also seen that when the surface of the rod is smooth, the coherence levels measured along the rod span are similar for the three downstream locations surveyed. For the gritted rod cases, larger variations are noted between the spanwise surveys performed at different downstream locations. When freestream turbulence is introduced, the spanwise coherence levels are only slightly reduced (and some coherence in the vortex shedding is maintained over a span of approximately 4D). This is consistent with Batham's study<sup>18</sup> which found that for the present flow regime, turbulence with integral scale greater than the rod diameter does not affect the cylinder flow. Based on the design of the turbulence grid used in this test,  $1 \leq T_s/D < 2$  for the 1/2" rod. Therefore only a portion of the eddies generated by the grid (as oppose to probably most of the eddies for the 1" rod test configurations) may be of a scale small enough to modify the cylinder flow and affect the spanwise coherence of the vortex shedding. This would explain the limited effect of the freestream turbulence on the spanwise coherence for the 1/2" rod cases compared to that for the 1" rod cases.

For model configurations 20 and 21 (1/2" rod with collars or wire wrap), the spanwise coherence of the vortex shedding was nonexistent for the spanwise surveys performed at 0.5" and 0.75" downstream of the rods. The cross spectra obtained for the 1/2" rod with collars (model configurations 21) are shown in Figure 37. For comparison, the cross spectra obtained between the stationary and traversing hot-wires for a simple 1/2" rod (model configurations 2) are displayed in figures 38 and 39. For configuration 2, the cross spectra are showing the expected correlation peaks at the vortex shedding frequency  $f_0$  and  $2f_0$ . For configuration 21 (as for configuration 20), the cross spectra do not show any correlation peaks for the spanwise surveys performed at  $x=0.5$ " and  $0.75$ ". For configuration 20, however, the spanwise coherence of the vortex shedding recovered at  $x=1.5$ ". This was not observed for the wire wrap configuration but it may be that the spanwise coherence of the vortex shedding may also recover further downstream of the rod, but just not at  $x=1.5$ ". Recovery in vortex shedding spanwise coherence downstream of the rod should not affect the level of radiated noise since the noise is generated by the flow (pressure) fluctuations that are occurring directly along the surface of the rod surface.

The noise spectra obtained for configurations 2, 20 and 21 from preliminary acoustic measurements show the drastic noise reduction that occurs when collars or the wire



wraps are installed on the rod. The noise spectra for 1/2" rod with smooth or gritted surface or equipped with collars or with a wire wrap are shown in Figure 40 for a uniform flow of Mach number 0.17. It is seen from this figure that good broadband noise reduction is achieved when the surface of the rod is gritted, however the spectral peak at the vortex shedding frequency is not attenuated. When the collars or the wire wrap are installed on the rod, about 25 dB reduction is achieved at the shedding frequency and the large tone generated by the vortex shedding is nearly eliminated. With the collar configuration, a 7 to 12 dB noise reduction is also achieved at frequencies greater than the vortex shedding frequency and up to 50 kHz (the cutoff frequency). The same level of noise reduction is achieved with the wire wrap between the shedding frequency and 18 kHz. Above 18 kHz, the noise reduction achieved is around 3 dB.

For model configuration 13 (rod with side plate) with smooth surface and immersed in a clean flow, the spanwise hot-wire measurements indicated only a very weak level of spanwise coherence in the vortex shedding. Thus, a coherence level of about 0.1 is maintained over a 4D span at the vortex shedding frequency  $f_0$  (for  $M=0.13$  and  $M=0.17$ ). Unlike the other model configurations tested, the hot-wire cross-spectra only displayed a (small) peak at  $f=f_0$ . This results from the fact that the hot-wire probes are located beside the plate, near the rod surface, and are therefore exposed to the vortices that are shed from only one side of the rod. When freestream turbulence is introduced, the measurements indicate an absence of spanwise coherence in the vortex shedding (at the survey location) for the smooth and gritted models.

## 5. Conclusion

PIV and hot-wire measurements performed in the wake of single and multiple rods configurations were presented. Measurements were taken for both smooth or gritted model surfaces, and with and without freestream turbulence. The effect of model surface treatment and freestream turbulence on the spanwise coherence of the vortex shedding was studied for several rod configurations. The results indicate that for a smooth rod and a flow Mach number of 0.13, the introduction of freestream turbulence led to a large reduction of the spanwise coherence of the vortex shedding when the turbulence integral scale  $T_s$  is less than the rod diameter  $D$ . For  $1 \leq T_s/D < 2$ , the freestream turbulence had limited effect on the coherence. It was also observed that freestream turbulence had minimal effect on the spanwise coherence of the vortex shedding for the gritted rods. For smooth and gritted rods, immersed in a clean flow, the spanwise coherence of the vortex shedding was found to scale well with Strouhal number.

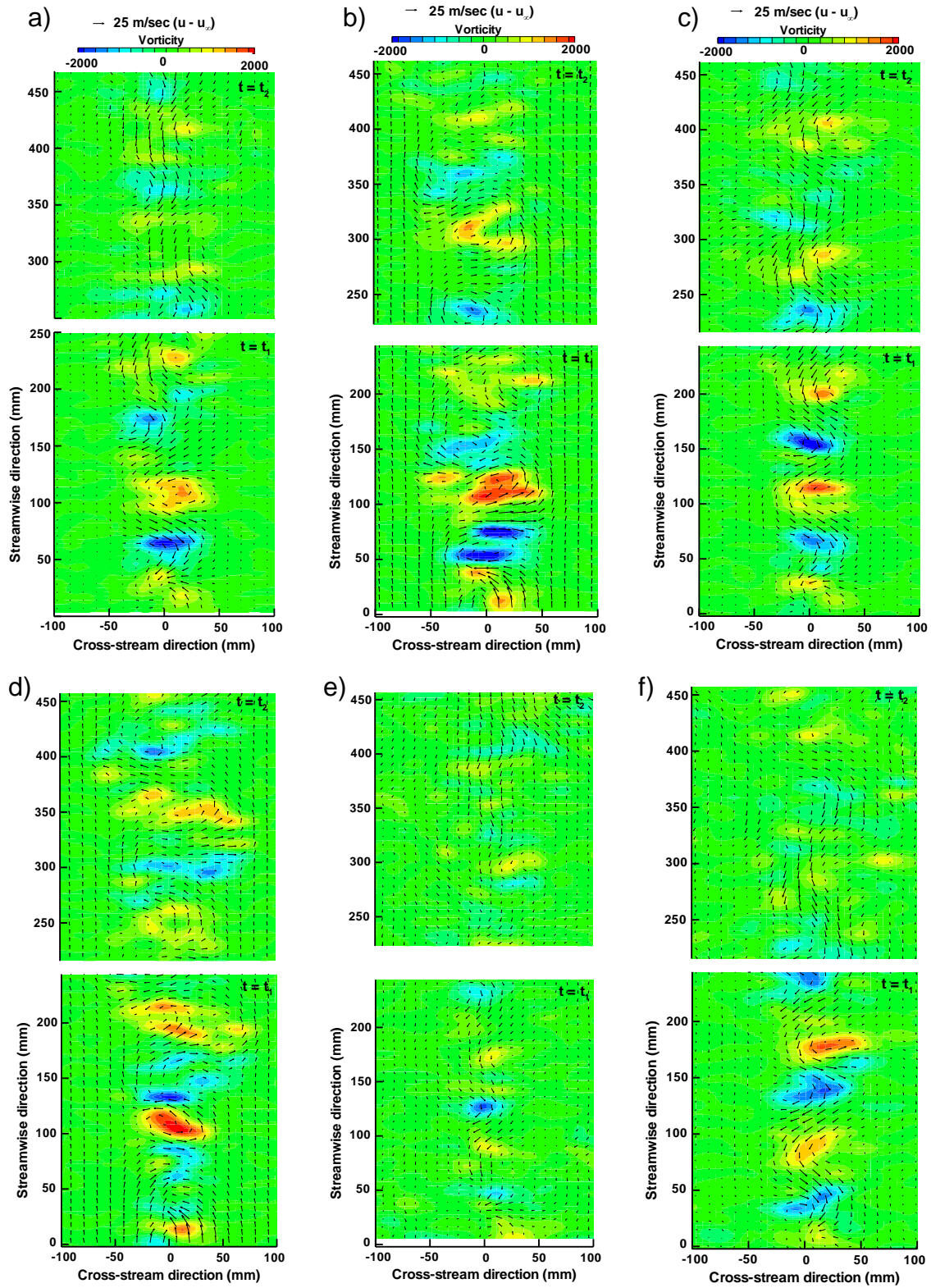
It was also verified that wrapping a wire or distributing collars along a rod successfully reduces the spanwise coherence of the vortex shedding, leading to a large noise reduction.

## References

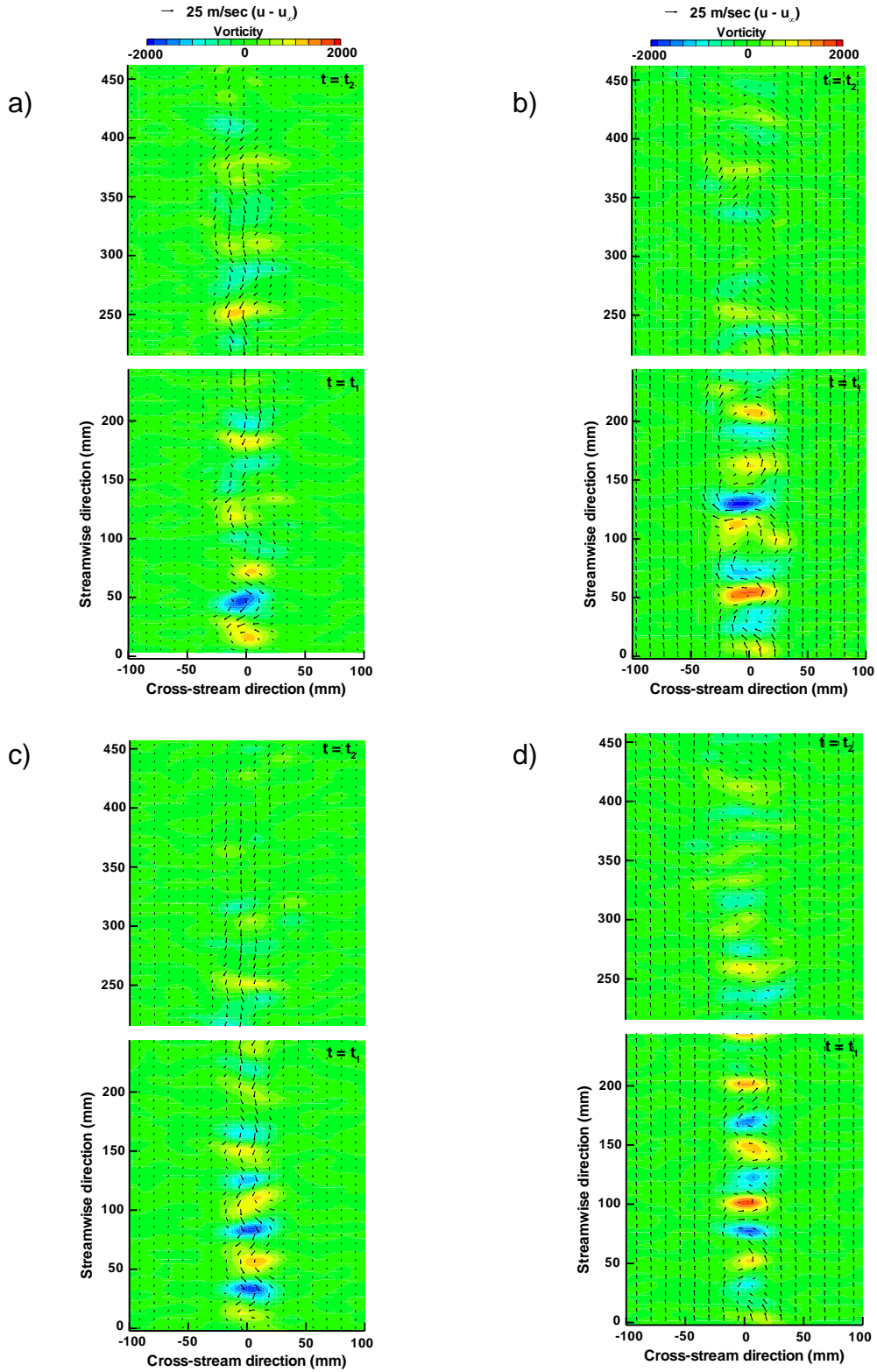
1. **Smith, M. G., Chow, L. C.** "Prediction method for aerodynamic noise from aircraft landing gear", AIAA paper 98-2228.

2. **Smith, M. G., Chow, L. C.** “Validation of a prediction model for aerodynamic noise from aircraft landing gear”, AIAA paper 2002-2581.
3. **Souliez, F. J., Long, L. N., Morris, P. J. and Sharma, A.** “Landing gear aerodynamic noise prediction using unstructured grids”, AIAA paper 2002-0799.
4. **Lockard, D. and Khorrami, M.** “Aeroacoustics analysis of a simplified landing gear”, AIAA paper 2003-3111.
5. **Guo, Y.** “A statistical model for landing gear noise prediction”, AIAA paper 2003-3227.
6. **Guo, Y., Yamamoto, K. and Stoker, R.** “An empirical model for landing gear noise prediction”, AIAA paper 2004-2888.
7. **Seror, C., Sagaut, p. and Belanger, A.** “ A numerical aeroacoustic analysis of a detailed landing gear” AIAA paper 2004-2884.
8. **Ravetta, P., Burdisso, R. and Ng, W.** “Wind tunnel aeroacoustic measurements of a 26%-scale 777 main landing gear”, AIAA paper 2004-2885.
9. **Jaeger, S., Burnside, N., Soderman, P., Horne, W. and James, K.** “Microphone array assessment of an isolated, 26%-scale, high-fidelity landing gear”, AIAA paper 2002-2410.
10. **Dobrzynski, W. and Buchholz, H.** “Full scale noise testing on airbus landing gears in the German Dutch wind tunnel”, AIAA Paper No. 97-1597.
11. **Dobrzynski, W., Chow, L., Guion, P., Shiells, D.** “Research into landing gear airframe noise reduction”, AIAA paper 2002-2409.
12. **Hutcheson, F. and Brooks, T.** “Noise Radiation from Single and Multiple Rod Configurations”, AIAA paper 2006-2629.
13. **Roach, P.** “The Generation of Nearly Isotropic Turbulence by Means of Grids”, Journal of Heat and Fluid Flow, Vol. 8, No. 2, June 1987.
14. **Ahuja, K. K., Martin, J., Miller, B. and Gu, X.** “On automobile antenna and roof rack noise control”, AIAA paper 93-
15. **Zdravkovich, M. M.** “Flow around circular cylinders, Volume 1”, Oxford University Press, 2003.
16. **Surry, D.** “Some effects of intense turbulence on the aerodynamics of a circular cylinder at subcritical Reynolds number”, Journal of Fluid Mechanics, Vol. 52, 543-563, 1972.

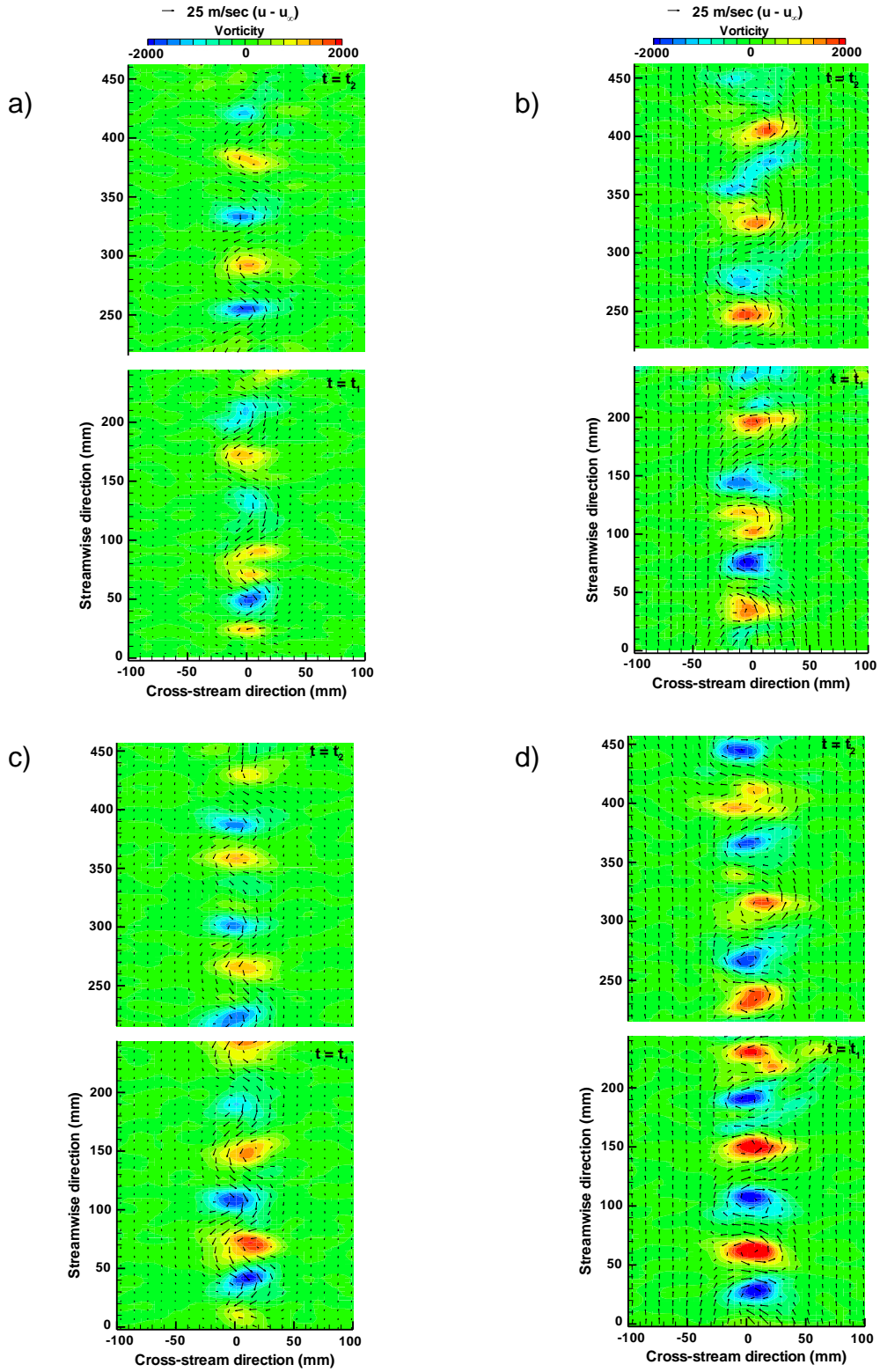
17. **Arie, M., Kiya, M., Suzuki, Y., Agino, M. and Takahashi, K.** “Characteristics of circular cylinders in turbulent flows”, Bulletin JSME, No. 24, 640-647, 1981.
18. **Batham, J. P.** “Pressure distribution on circular cylinders at critical Reynolds numbers”, Journal of Fluid Mechanics, Vol. 57, 209-28, 1973.
19. **Zdravkovich, M. M.** “Flow around circular cylinders, Volume 2”, Oxford University Press, 1997.



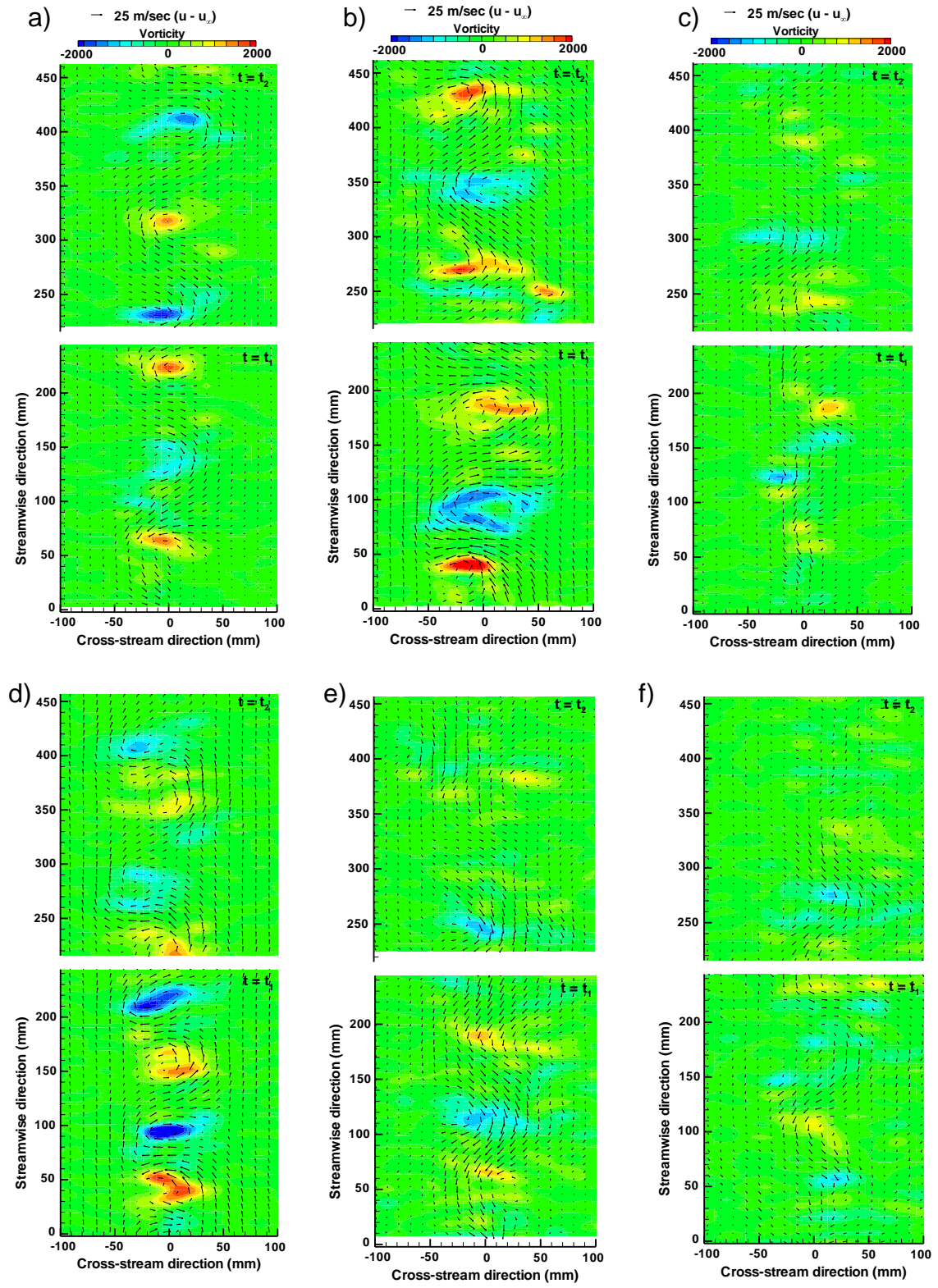
**Figure 7.** Configuration 1 (1" diameter rod). Axial vorticity contours and in-plane velocity vectors .  
**a)** smooth rod, clean flow,  $M=0.13$ ; **b)** smooth rod, clean flow,  $M=0.17$ ; **c)** gritted rod, clean flow,  $M=0.13$ ; **d)** gritted rod, clean flow,  $M=0.17$  **e)** smooth rod, turbulent flow,  $M=0.13$ ; **f)** gritted rod, turbulent flow,  $M=0.13$ .



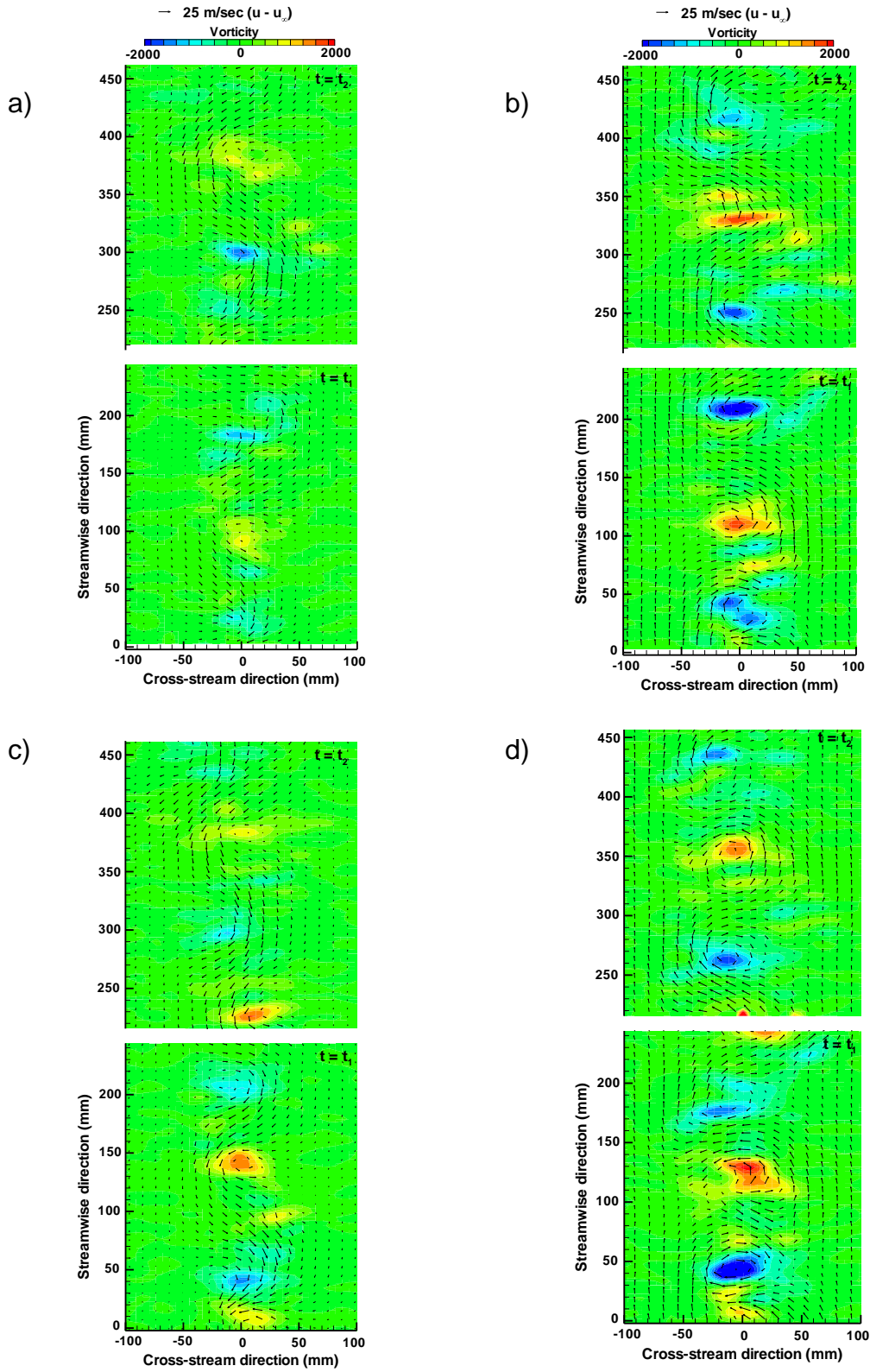
**Figure 8.** Configuration 2 (1/2" diameter rod). Axial vorticity contours and in-plane velocity vectors. Clean flow. **a)** smooth rod,  $M=0.13$ ; **b)** smooth rod,  $M=0.17$ ; **c)** gritted rod,  $M=0.13$ ; **d)** gritted rod,  $M=0.17$ .



**Figure 9.** Configuration 3 (two 1" diameter rods together, streamwise alignment). Axial vorticity contours and in-plane velocity vectors. Clean flow. **a)** smooth rod,  $M=0.13$ ; **b)** smooth rod,  $M=0.17$ ; **c)** gritted rod,  $M=0.13$ ; **d)** gritted rod,  $M=0.17$ .

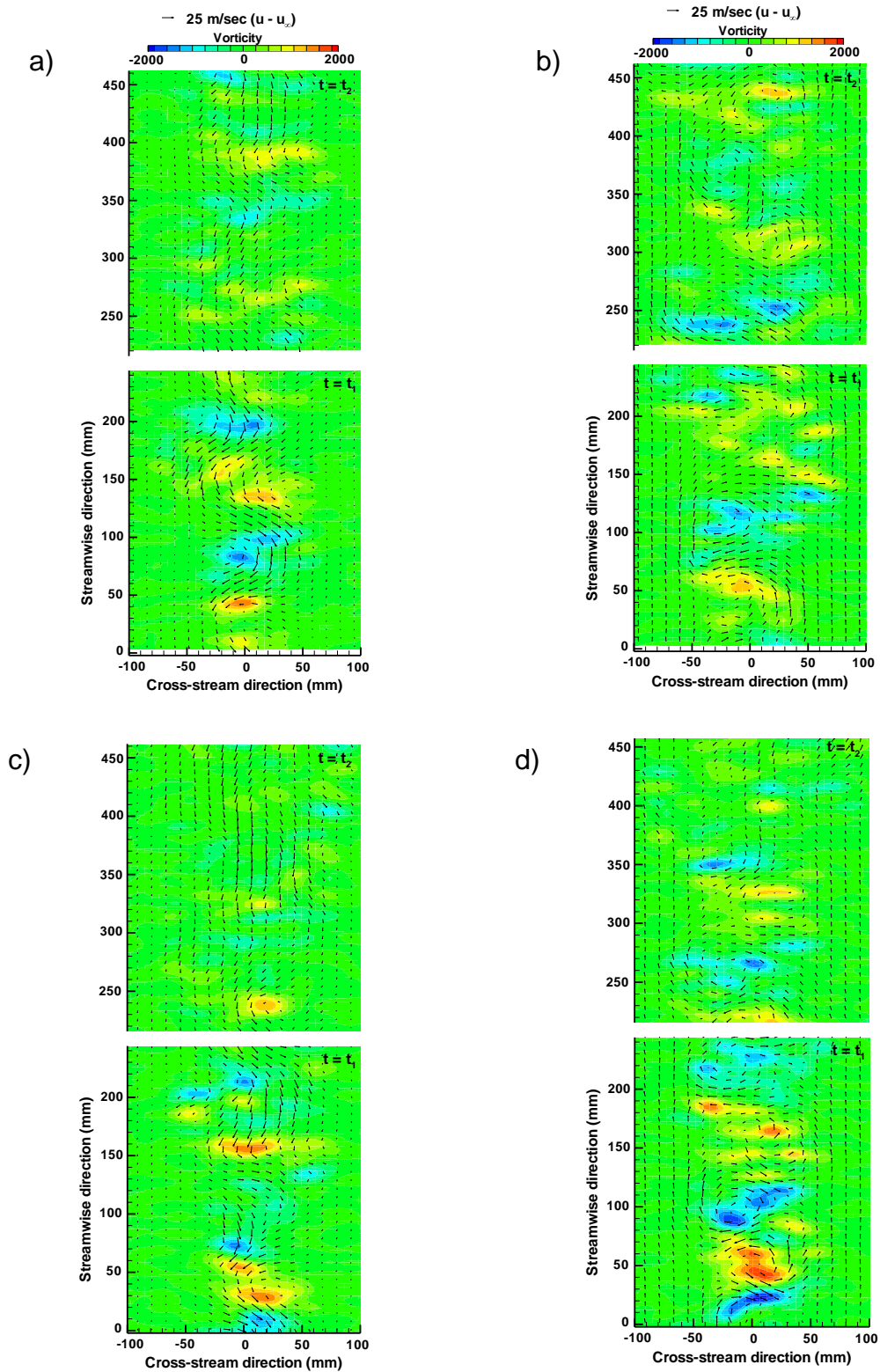


**Figure 10.** Configuration 4 (two 1" diameter rods, 2" apart, streamwise alignment). Axial vorticity contours and in-plane velocity vectors. **a)** smooth rod, clean flow,  $M=0.13$ ; **b)** smooth rod, clean flow,  $M=0.17$ ; **c)** gritted rod, clean flow,  $M=0.13$ ; **d)** gritted rod, clean flow,  $M=0.17$ ; **e)** smooth rod, turbulent flow,  $M=0.13$ ; **f)** gritted rod, turbulent flow,  $M=0.13$ .

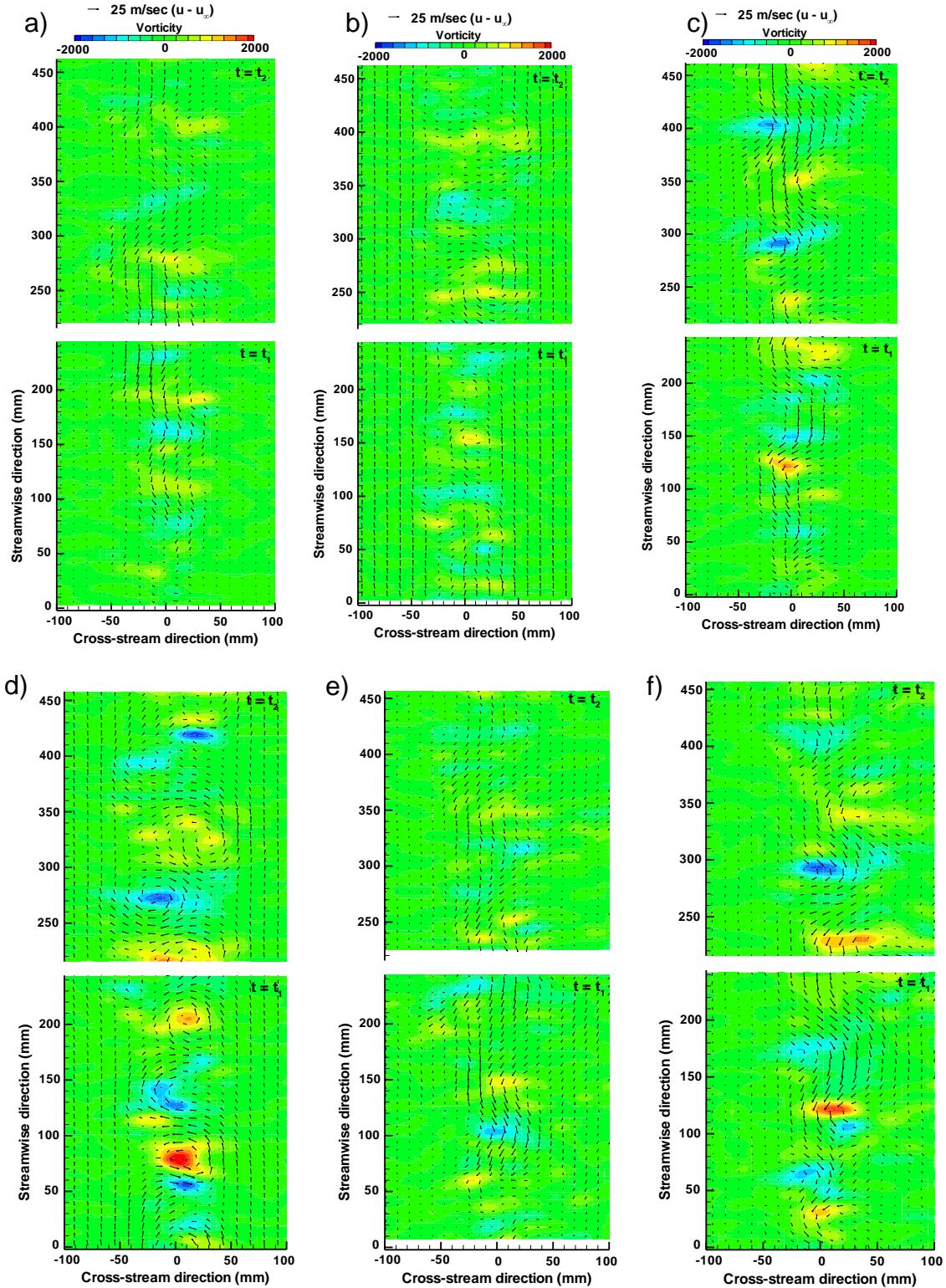


**Figure 11.** Configuration 5 (two 1" diameter rods, 3" apart, streamwise alignment). Axial vorticity contours and in-plane velocity vectors. Clean flow. **a)** smooth rod,  $M=0.13$ ; **b)** smooth rod,  $M=0.17$ ; **c)** gritted rod,  $M=0.13$ ; **d)** gritted rod,  $M=0.17$ .

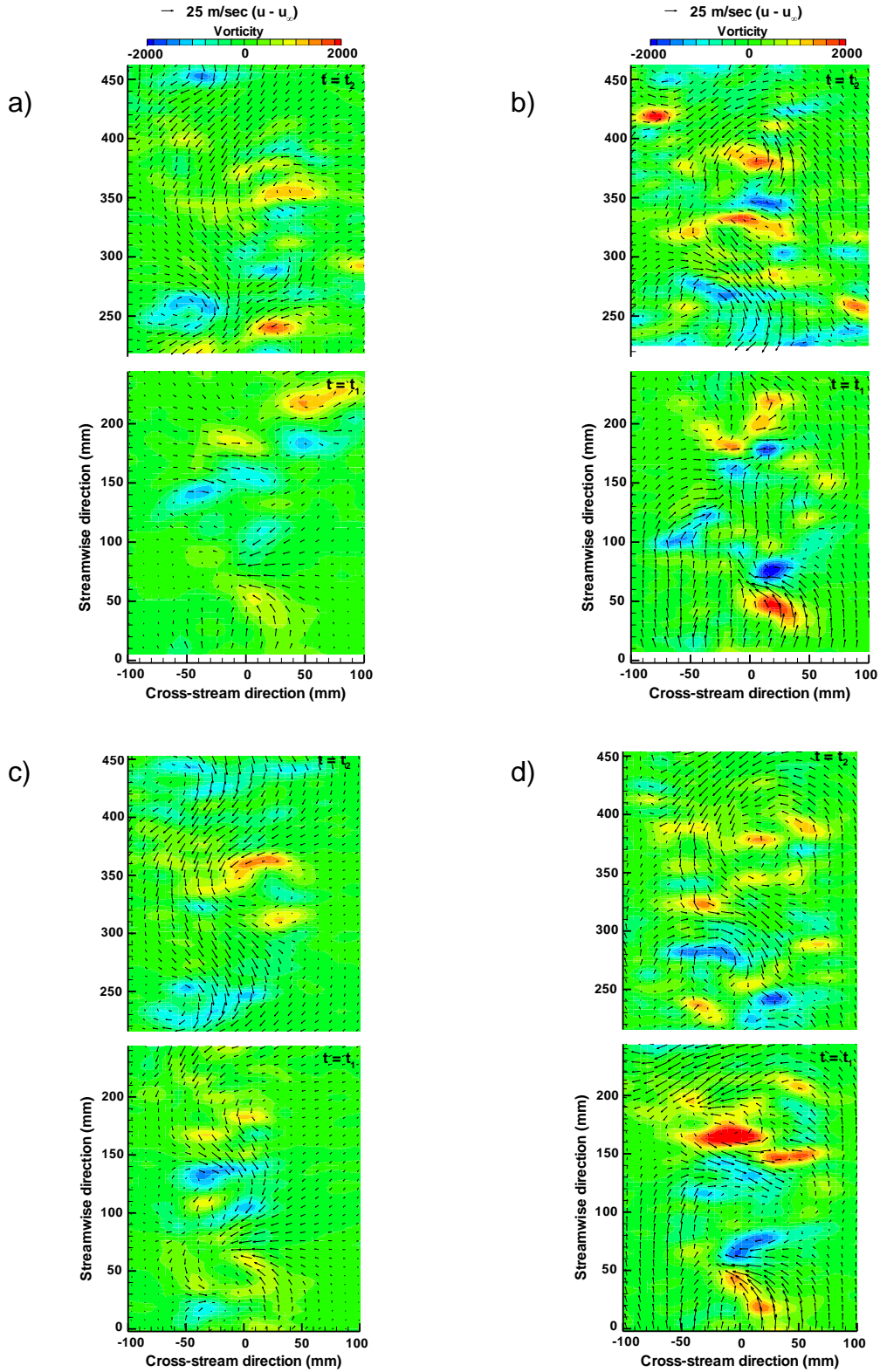




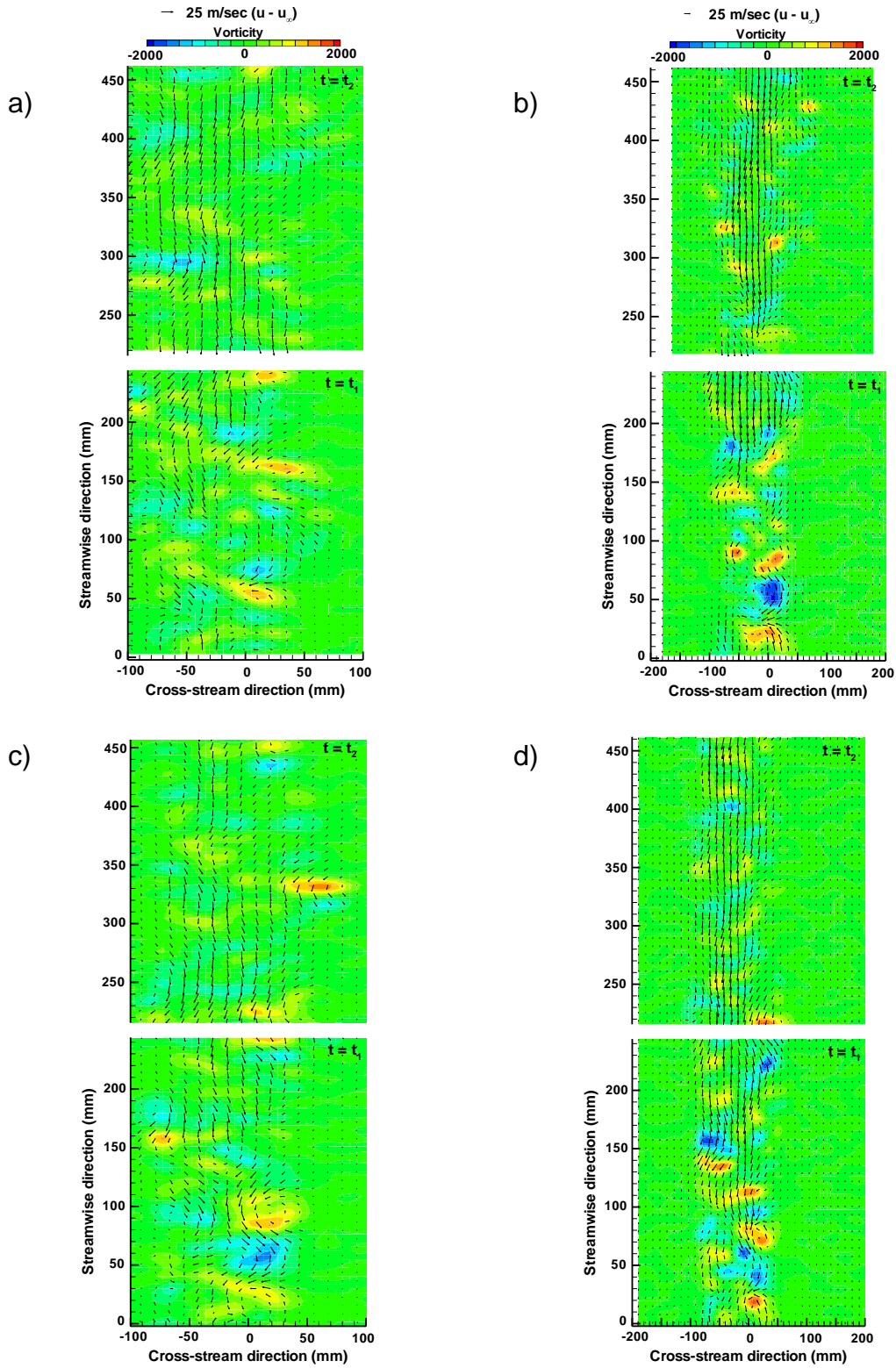
**Figure 12.** Configuration 6 ( $\frac{1}{2}$ " rod downstream of 1" rod). Axial vorticity contours and in-plane velocity vectors. Clean Flow. **a)** smooth rod,  $M=0.13$ ; **b)** smooth rod,  $M=0.17$ ; **c)** gritted rod,  $M=0.13$ ; **d)** gritted rod,  $M=0.17$ .



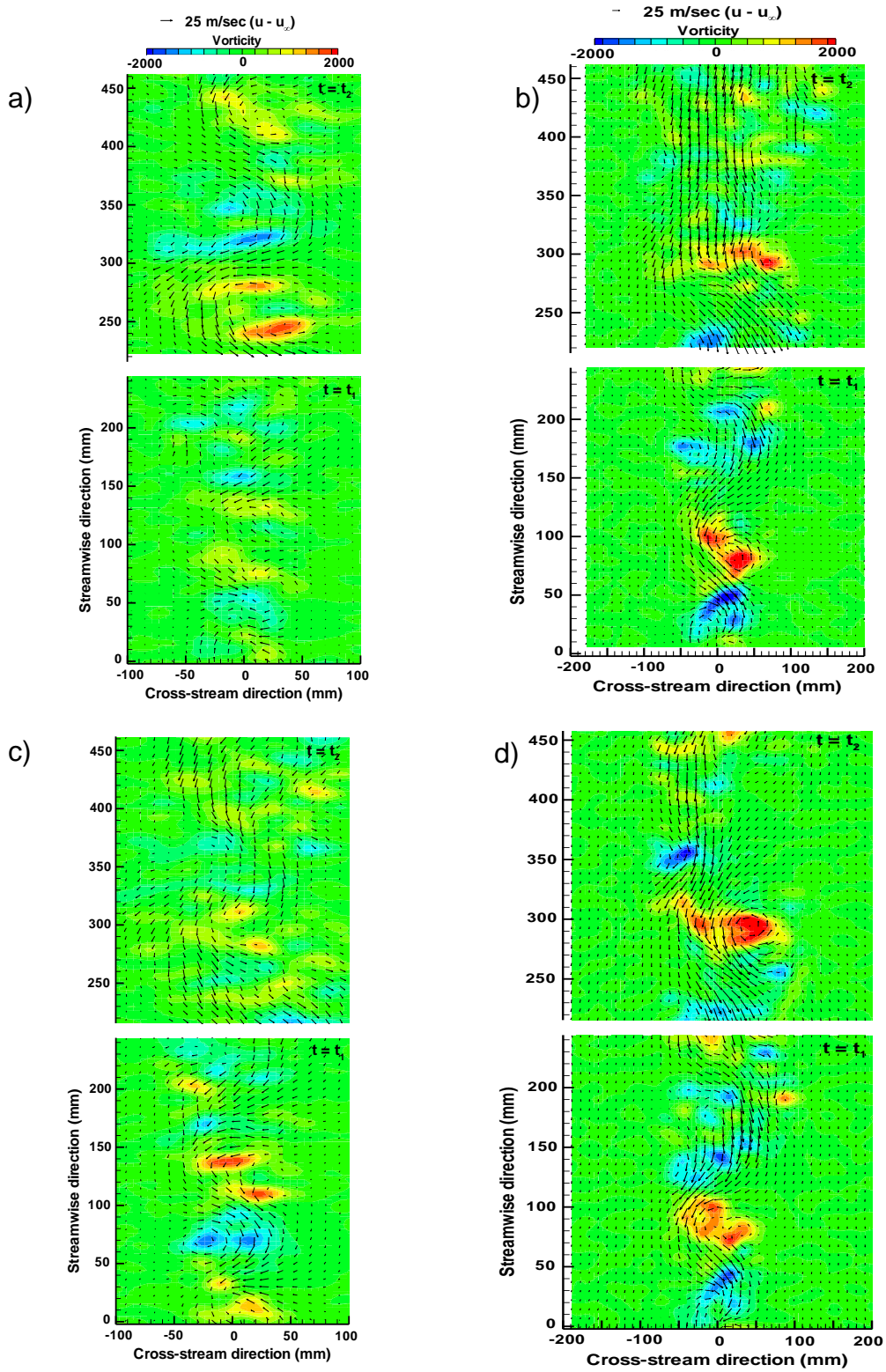
**Figure 13.** Configuration 7 (1" rod downstream of 1/2" rod). Axial vorticity contours and in-plane velocity vectors. **a)** smooth rod, clean flow,  $M=0.13$ ; **b)** smooth rod, clean flow,  $M=0.17$ ; **c)** gritted rod, clean flow,  $M=0.13$ ; **d)** gritted rod, clean flow,  $M=0.17$ ; **e)** smooth rod, turbulent flow,  $M=0.13$ ; **f)** gritted rod, turbulent flow,  $M=0.13$ .



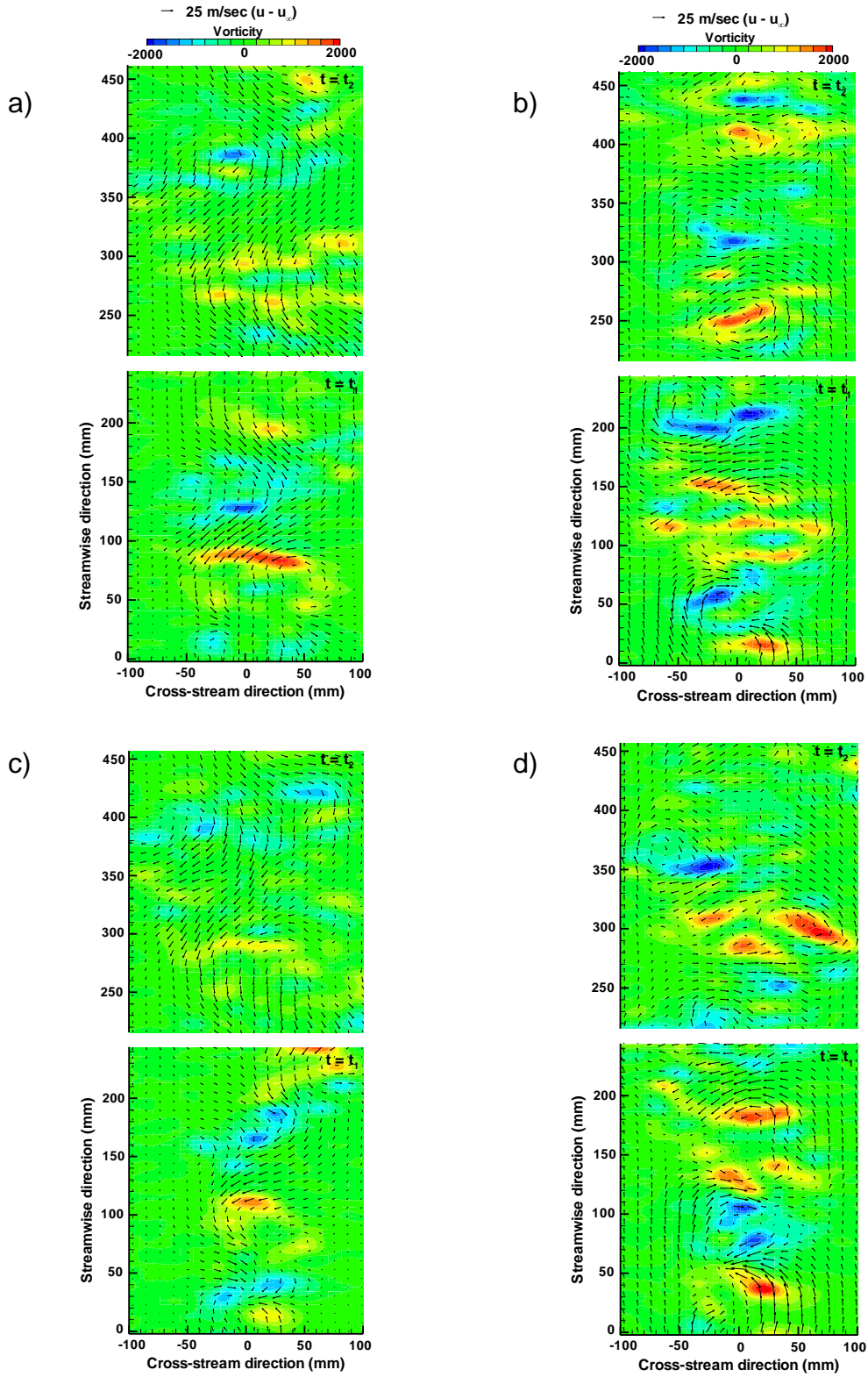
**Figure 14.** Configuration 8 (two 1" diameter rods together, cross-stream alignment). Axial vorticity contours and in-plane velocity vectors. Clean flow. **a)** smooth rod,  $M=0.13$ ; **b)** smooth rod,  $M=0.17$ ; **c)** gritted rod,  $M=0.13$ ; **d)** gritted rod,  $M=0.17$ .



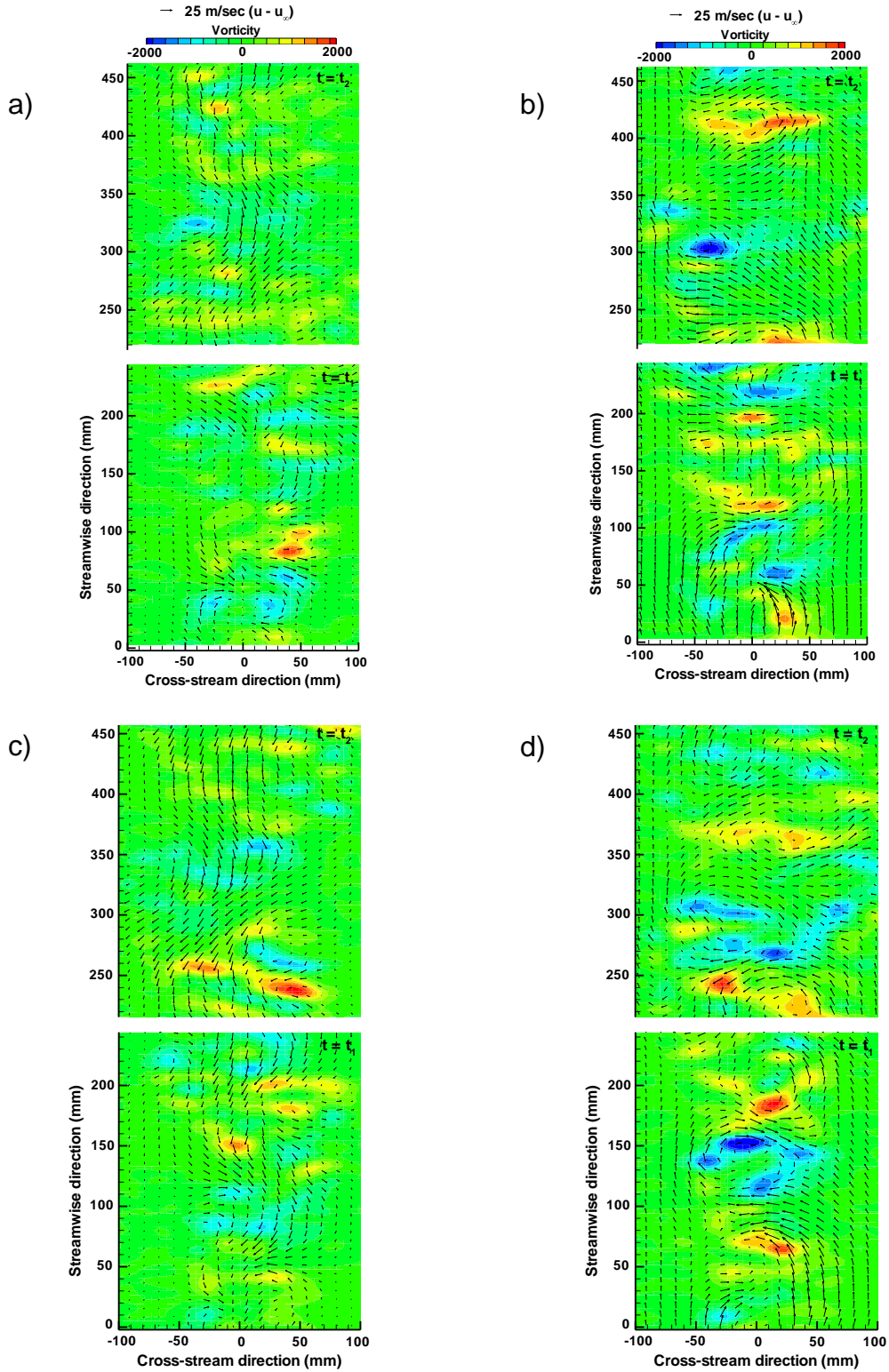
**Figure 15.** Configuration 9 (two 1" diameter rods, 2" apart, cross-stream alignment). Axial vorticity contours and in-plane velocity vectors. Clean flow. **a)** smooth rod,  $M=0.13$ ; **b)** smooth rod,  $M=0.17$ ; **c)** gritted rod,  $M=0.13$ ; **d)** gritted rod,  $M=0.17$ .



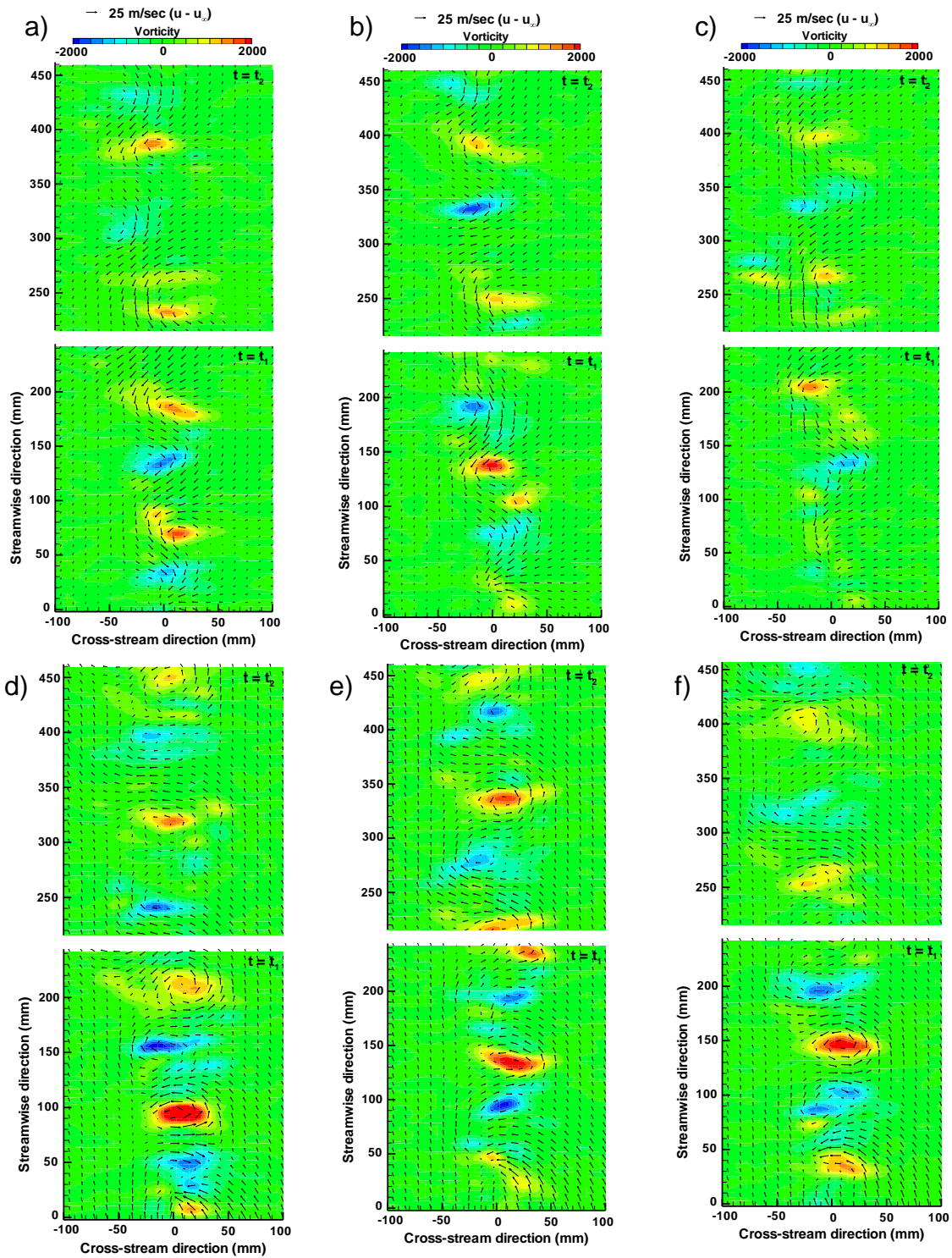
**Figure 16.** Configuration 10 (square bar). Axial vorticity contours and in-plane velocity vectors. Clean flow **a)** smooth rod,  $M=0.13$ ; **b)** smooth rod,  $M=0.17$ ; **c)** gritted rod,  $M=0.13$ ; **d)** gritted rod,  $M=0.17$ .



**Figure 17.** Configuration 11 (square bar, rotated  $30^\circ$ ). Axial vorticity contours and in-plane velocity vectors. Clean flow. **a)** smooth rod,  $M=0.13$ ; **b)** smooth rod,  $M=0.17$ ; **c)** gritted rod,  $M=0.13$ ; **d)** gritted rod,  $M=0.17$ .

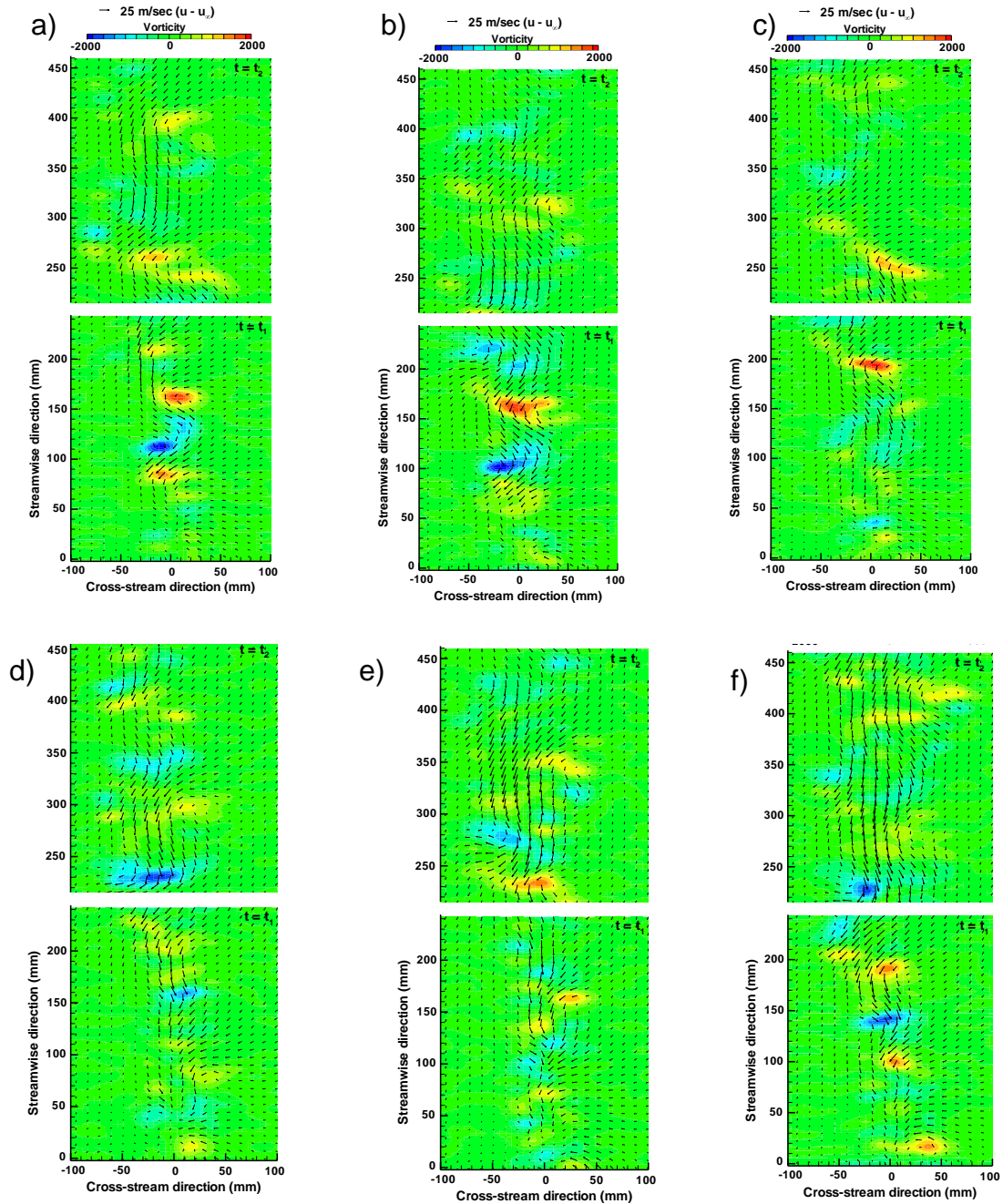


**Figure 18.** Configuration 12 (square bar, rotated  $45^\circ$ ). Axial vorticity contours and in-plane velocity vectors. Clean flow. **a)** smooth rod,  $M=0.13$ ; **b)** smooth rod,  $M=0.17$ ; **c)** gritted rod,  $M=0.13$ ; **d)** gritted rod,  $M=0.17$ .

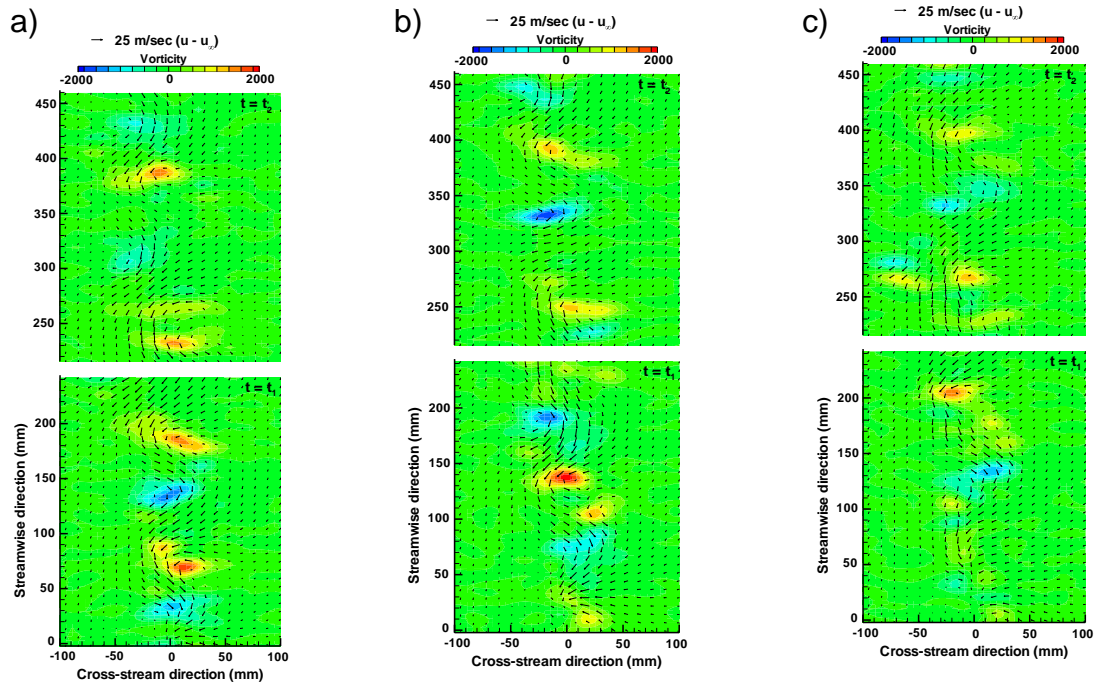


**Figure 19a.** Configuration 13 (1" rod with plate, no gap). Axial vorticity contours and in-plane velocity vectors. Smooth model surface, clean flow. Measurements performed at the following spanwise locations **a)** center of a bracket,  $M=0.13$ ; **b)** bracket side edge,  $M=0.13$ ; **c)** between two brackets,  $M=0.13$ ; **d)** center of a bracket,  $M=0.17$ ; **e)** bracket side edge,  $M=0.17$ ; **f)** between two brackets,  $M=0.17$ .

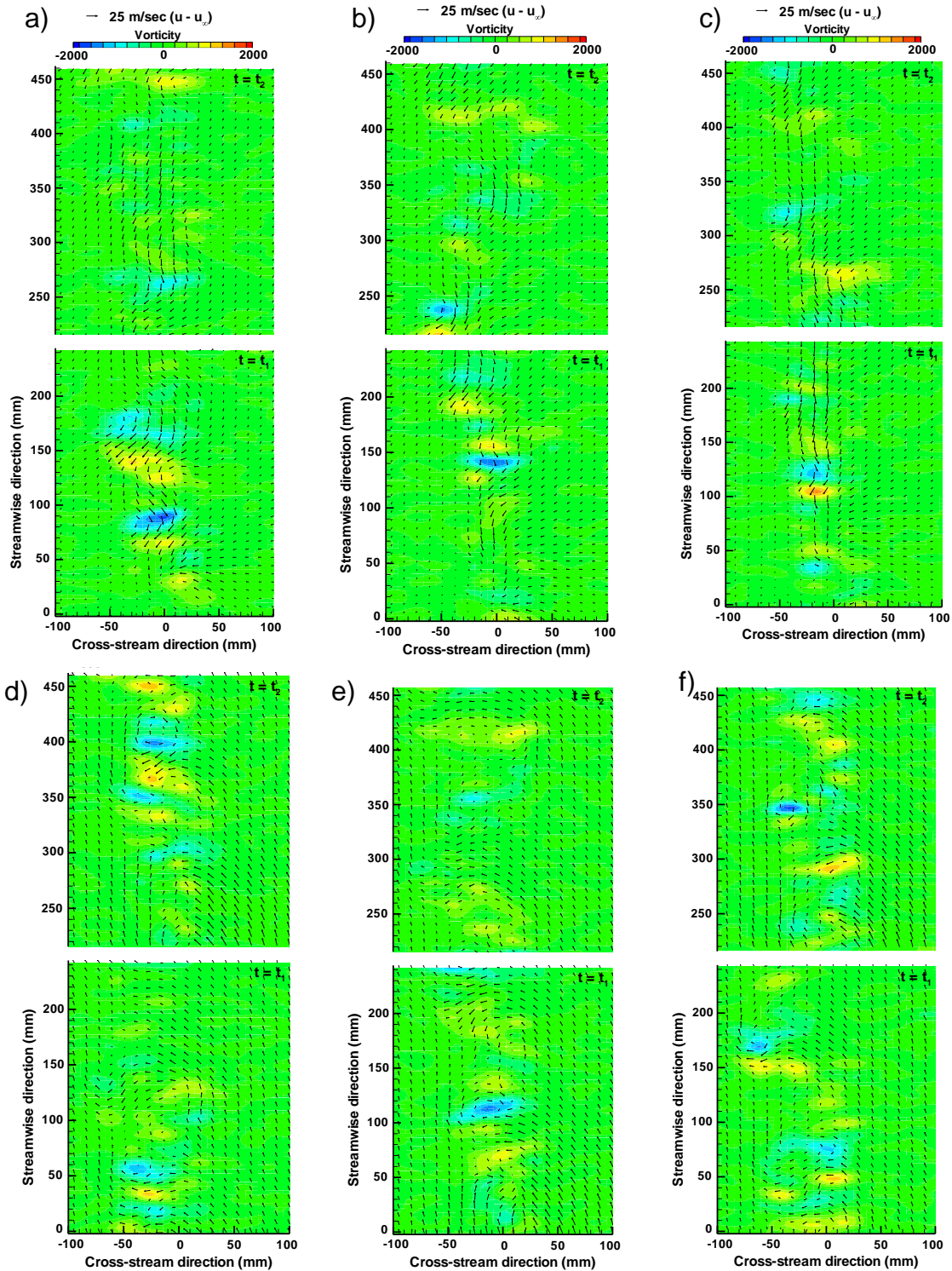




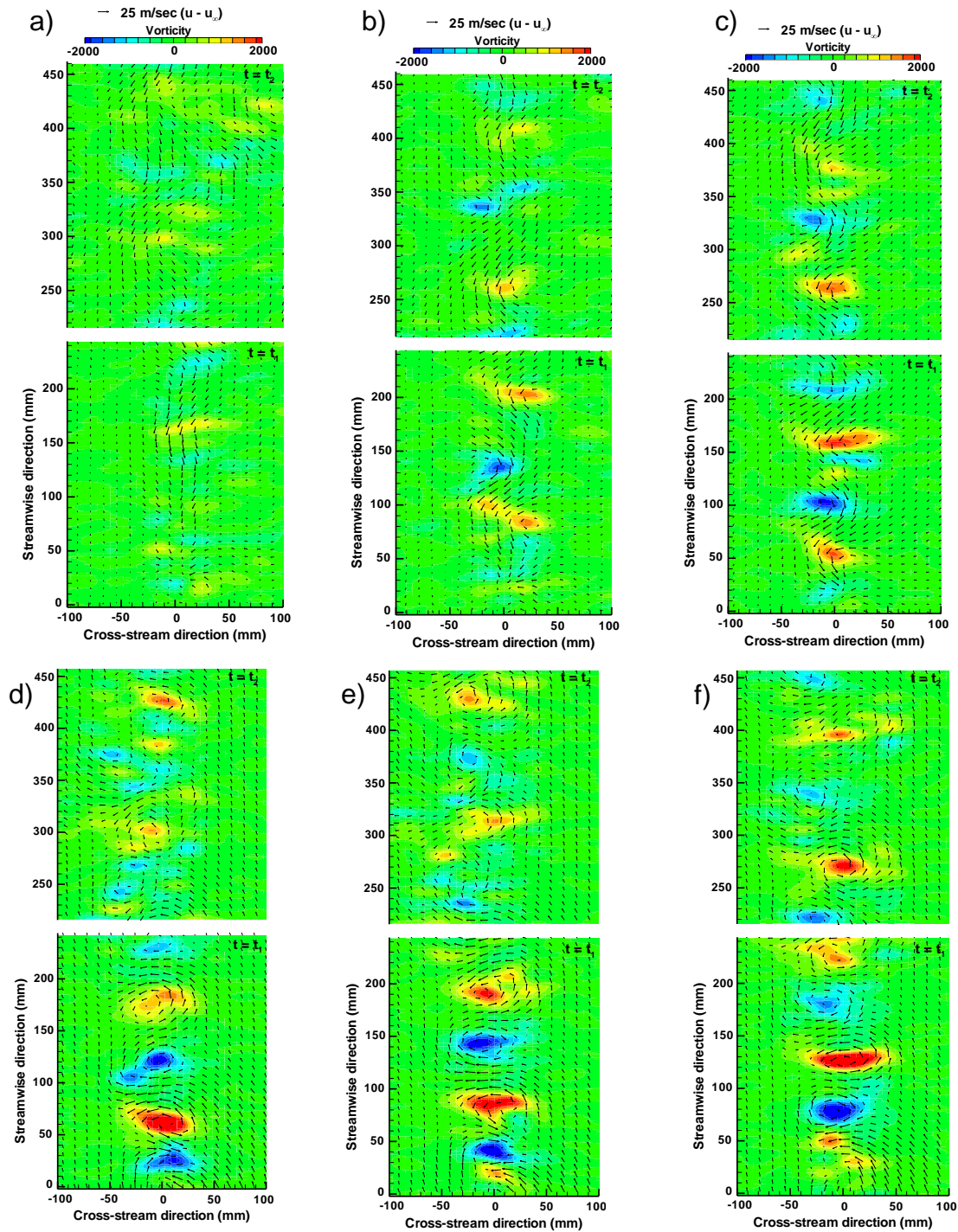
**Figure 19b.** Configuration 13 (1" rod with plate, no gap). Axial vorticity contours and in-plane velocity vectors. Gridded model, clean flow. Measurements performed at the following spanwise locations **a)** center of a bracket,  $M=0.13$ ; **b)** bracket side edge,  $M=0.13$ ; **c)** between two brackets,  $M=0.13$ ; **d)** center of a bracket,  $M=0.17$ ; **e)** bracket side edge,  $M=0.17$ ; **f)** between two brackets,  $M=0.17$ .



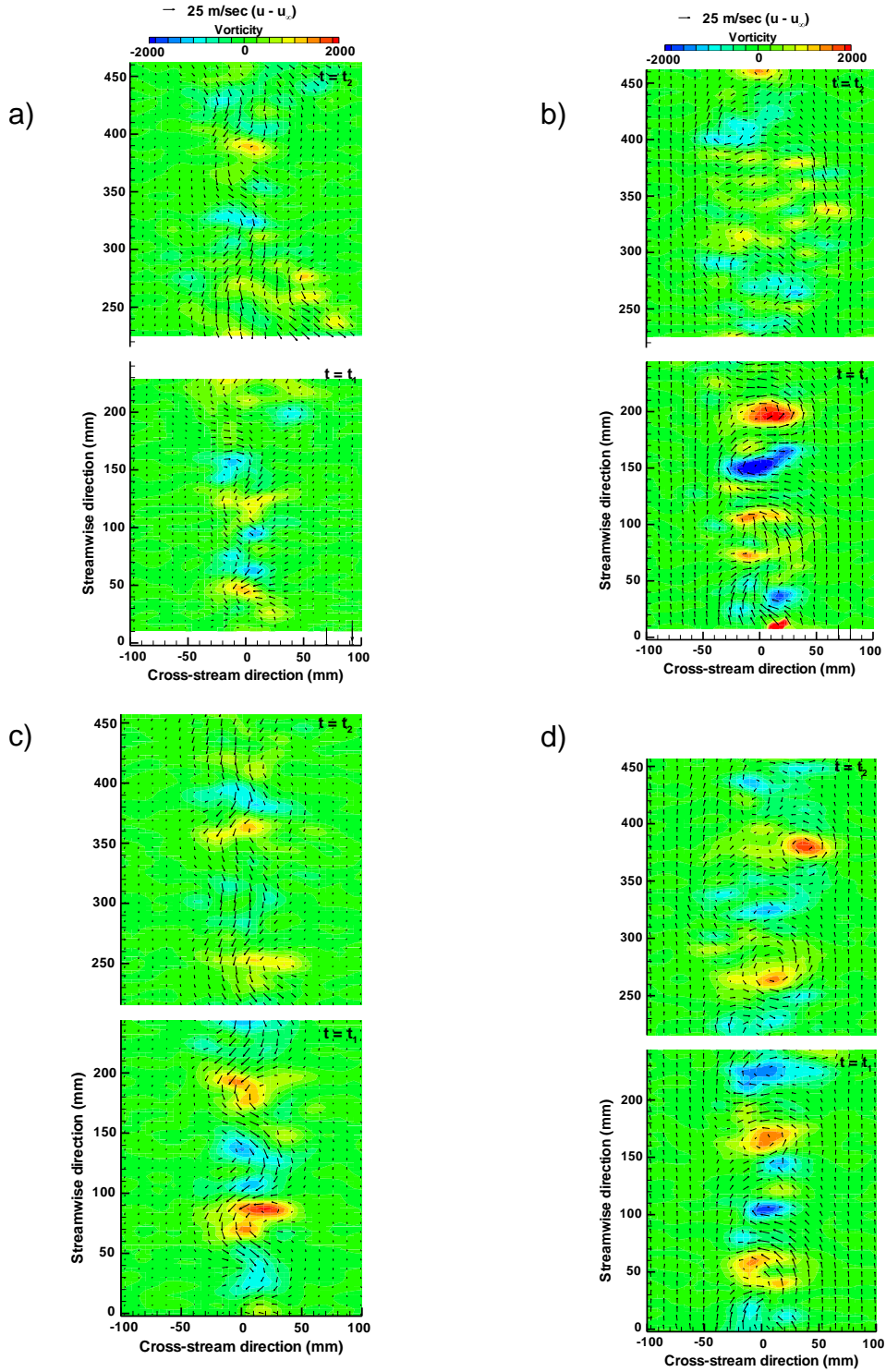
**Figure 19c.** Configuration 13 (1" rod with plate, no gap). Axial vorticity contours and in-plane velocity vectors. Gridded model, turbulent flow. Measurements performed at the following spanwise locations **a)** center of a bracket,  $M=0.13$ ; **b)** side edge of a bracket,  $M=0.13$ ; **c)** between two brackets,  $M=0.13$ ;



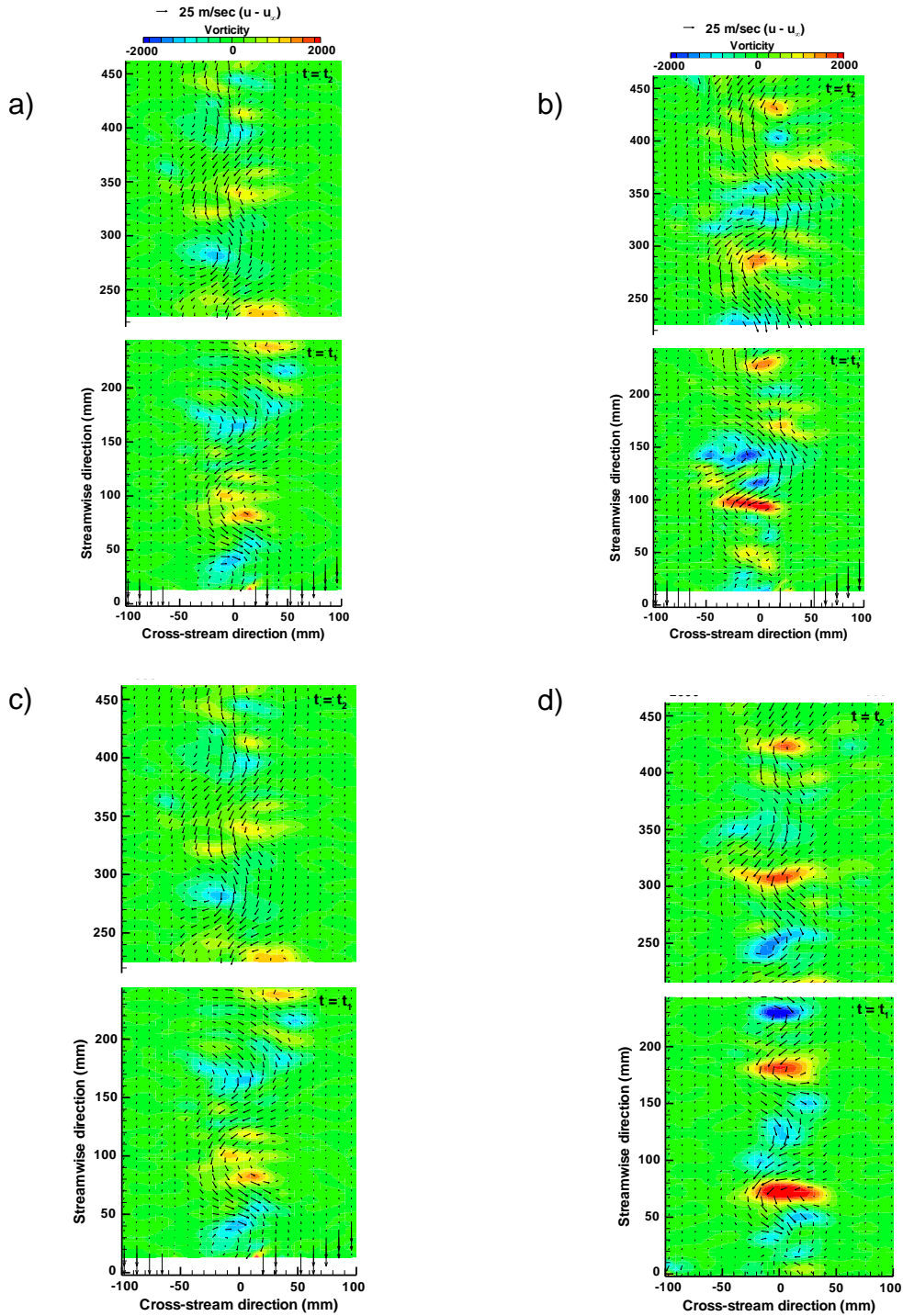
**Figure 20a.** Configuration 14 (1" rod with plate, 0.1" gap). Axial vorticity contours and in-plane velocity vectors. Smooth model, clean flow. Measurements performed at the following spanwise locations **a)** center of a bracket,  $M=0.13$ ; **b)** bracket side edge,  $M=0.13$ ; **c)** between two brackets,  $M=0.13$ ; **d)** center of a bracket,  $M=0.17$ ; **e)** bracket side edge,  $M=0.17$ ; **f)** between two brackets,  $M=0.17$ .



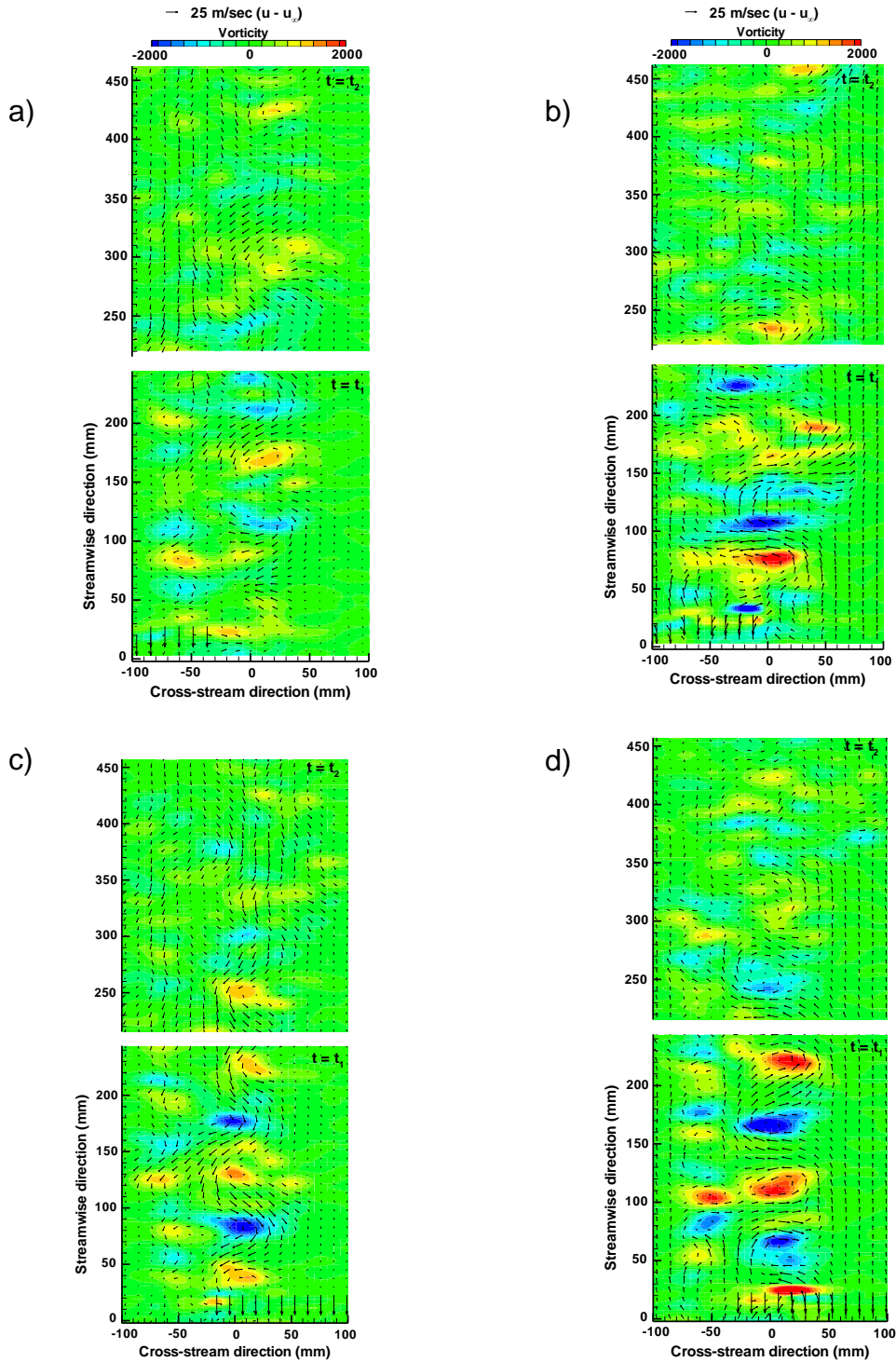
**Figure 20b.** Configuration 14 (1" rod with plate, 0.1" gap). Axial vorticity contours and in-plane velocity vectors. Gridded model, clean flow. Measurements performed at the following spanwise locations **a)** center of a bracket,  $M=0.13$ ; **b)** bracket side edge,  $M=0.13$ ; **c)** between two brackets,  $M=0.13$ ; **d)** center of a bracket,  $M=0.17$ ; **e)** bracket side edge,  $M=0.17$ ; **f)** between two brackets,  $M=0.17$ .



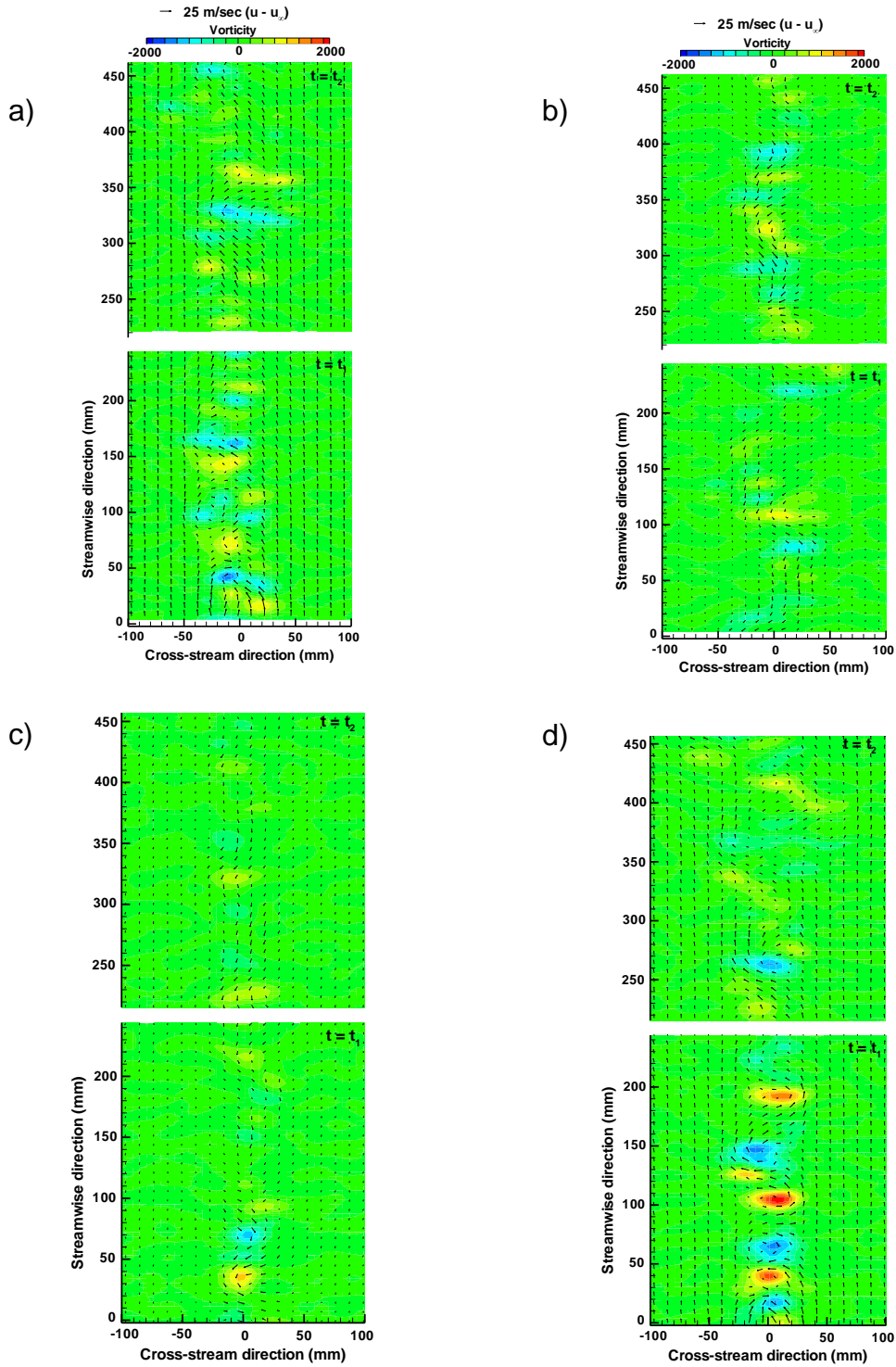
**Figure 21.** Configuration 15 (1" rod, 15° with flow). Axial vorticity contours and in-plane velocity vectors. Clean flow. **a)** smooth rod,  $M=0.13$ ; **b)** smooth rod,  $M=0.17$ ; **c)** gridded rod,  $M=0.13$ ; **d)** gridded rod,  $M=0.17$ .



**Figure 22.** Configuration 16 (1" rod, 30° with flow). Axial vorticity contours and in-plane velocity vectors. Clean flow. **a)** smooth rod,  $M=0.13$ ; **b)** smooth rod,  $M=0.17$ ; **c)** gritted rod,  $M=0.13$ ; **d)** gritted rod,  $M=0.17$ .

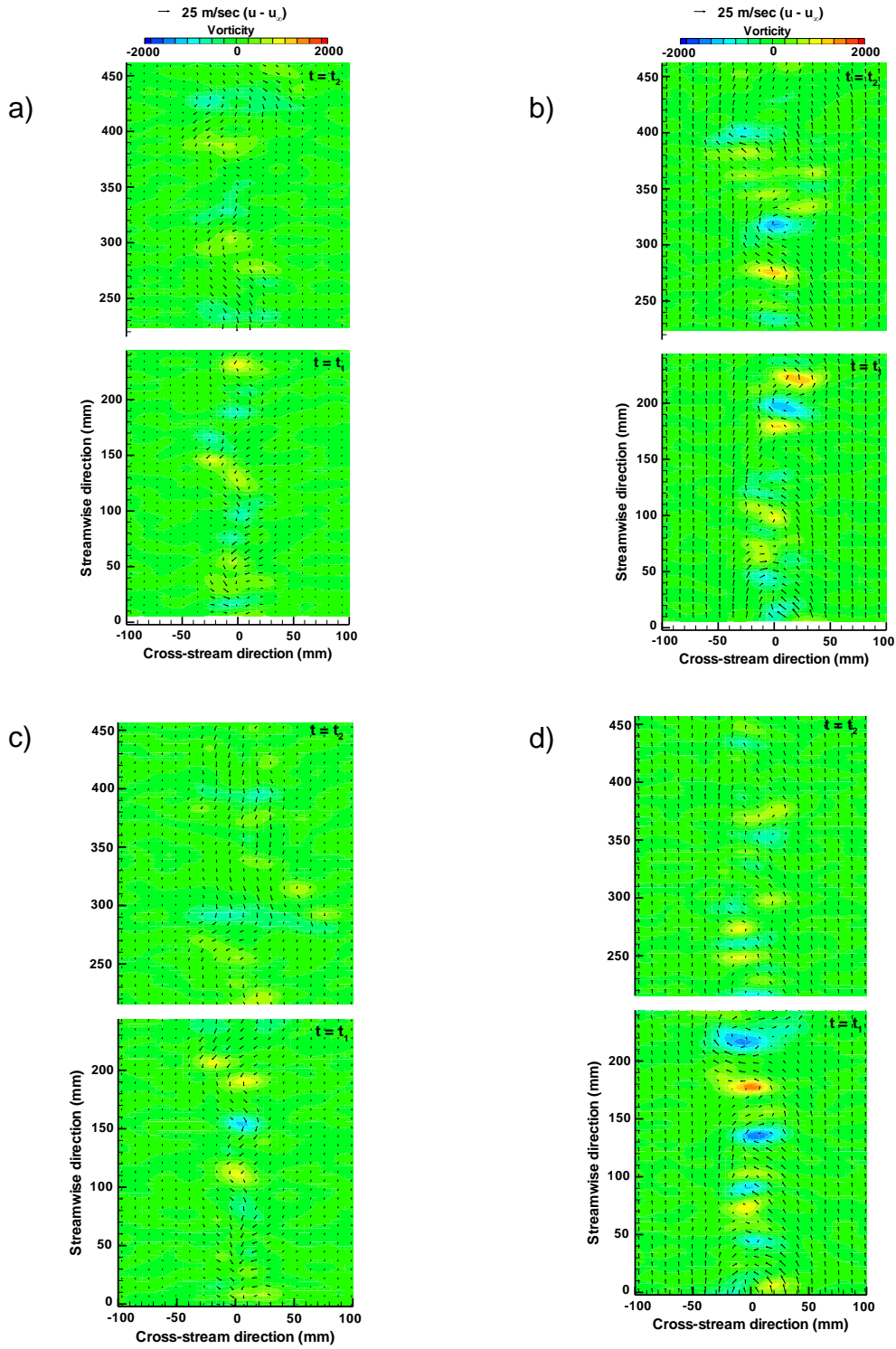


**Figure 23.** Configuration 17 (1" rod and 1/2" rod 30° with flow). Axial vorticity contours and in-plane velocity vectors. Clean flow. **a)** smooth rod,  $M=0.13$ ; **b)** smooth rod,  $M=0.17$ ; **c)** gritted rod,  $M=0.13$ ; **d)** gritted rod,  $M=0.17$ .

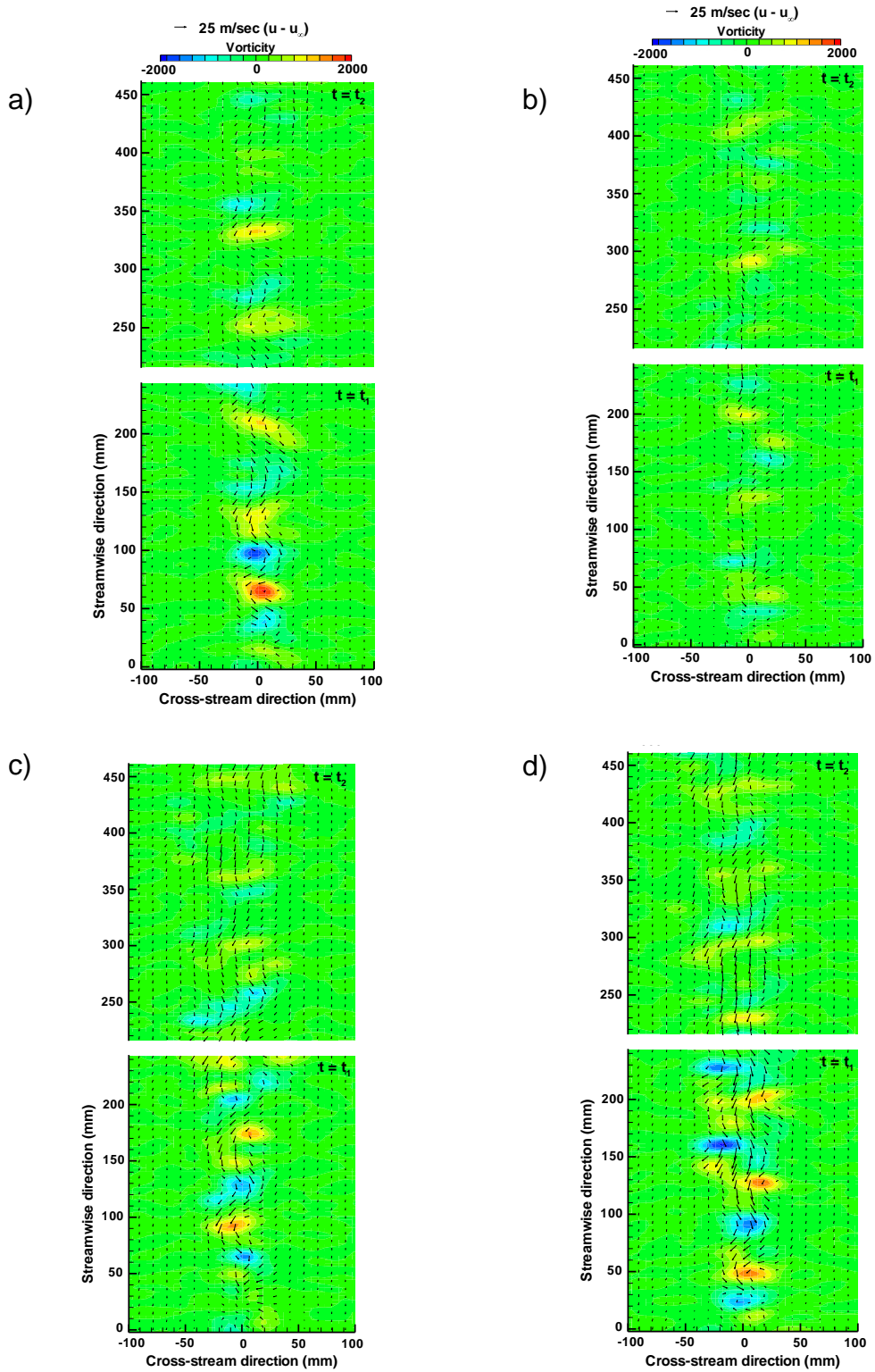


**Figure 24.** Configuration 18 (1/2" rod with 1 rounded collar). Axial vorticity contours and in-plane velocity vectors. Clean flow. **a)** smooth rod,  $M=0.13$ ; **b)** smooth rod,  $M=0.17$ ; **c)** gritted rod,  $M=0.13$ ; **d)** gritted rod,  $M=0.17$ .

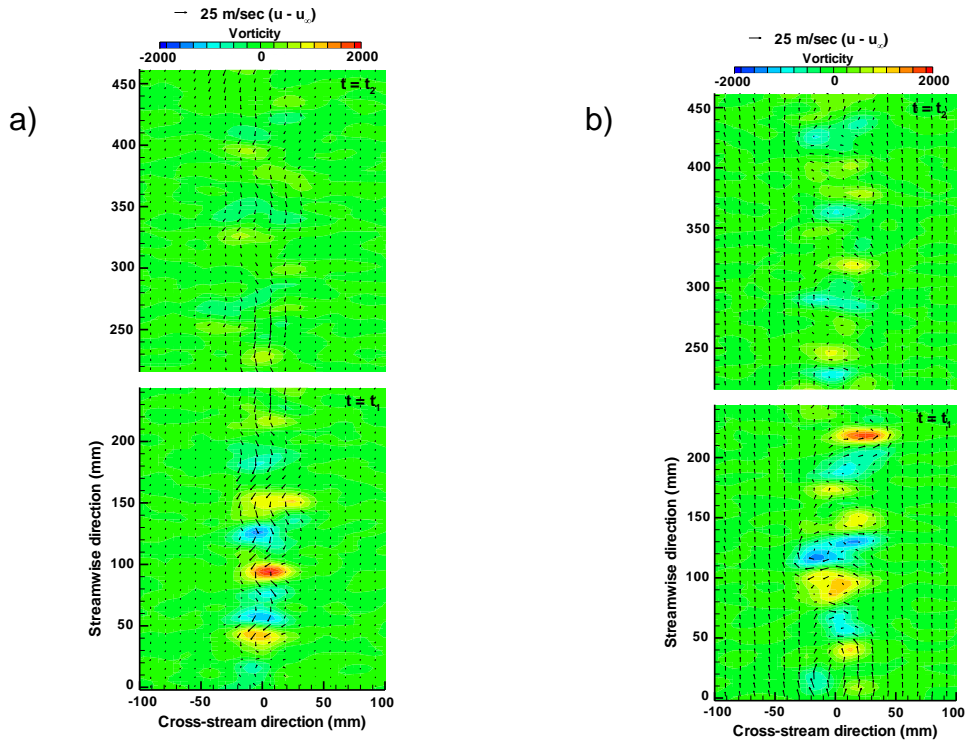




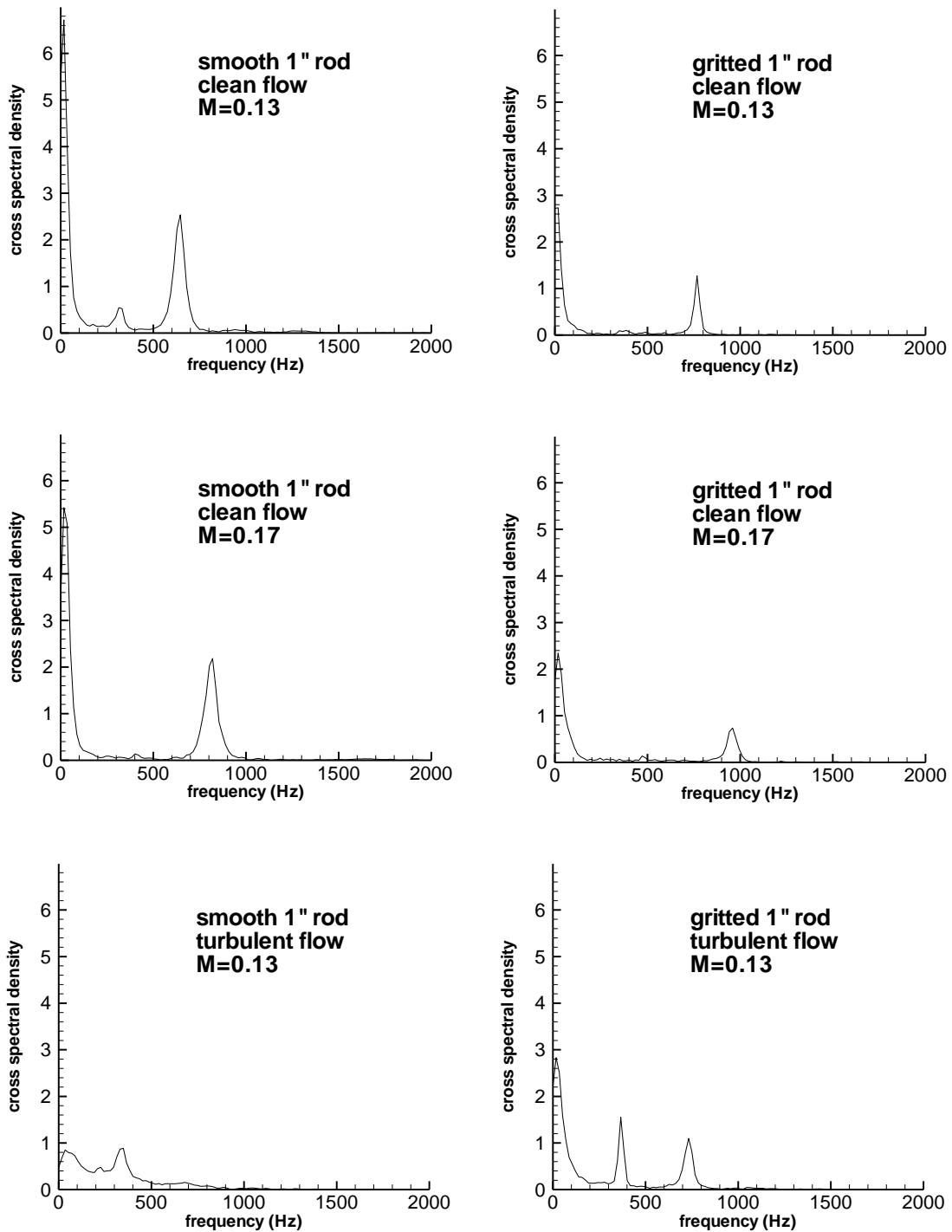
**Figure 25.** Configuration 19 (1" rod with square collar). Axial vorticity contours and in-plane velocity vectors. Clean flow. **a)** smooth rod,  $M=0.13$ ; **b)** smooth rod,  $M=0.17$ ; **c)** gritted rod,  $M=0.13$ ; **d)** gritted rod,  $M=0.17$ .



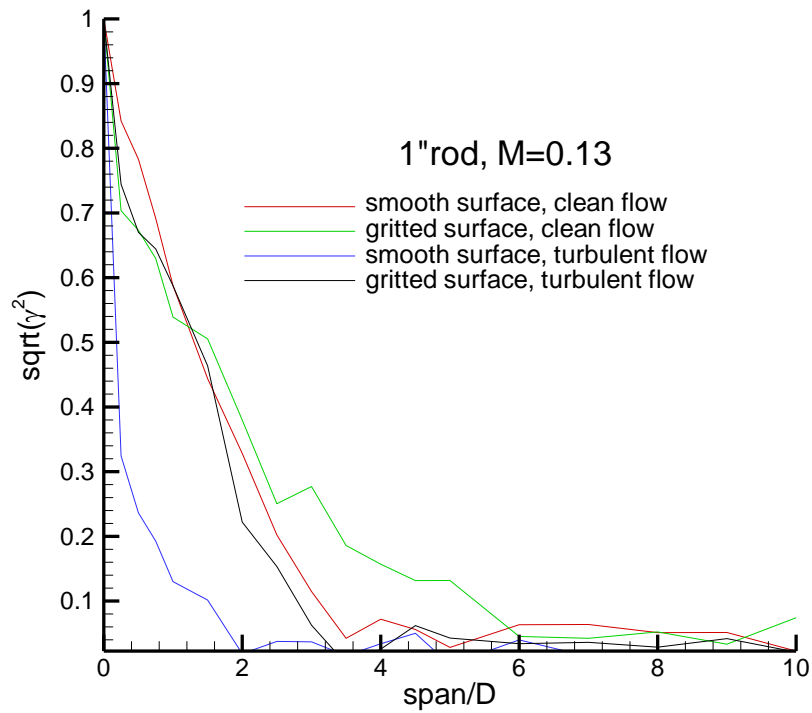
**Figure 26.** Configuration 20 (1" rod with 11 collars). Axial vorticity contours and in-plane velocity vectors. Smooth model, clean flow. Spanwise location of measurements and flow speed: **a)** at center of a collar,  $M=0.13$ ; **b)** midway between two collars),  $M=0.13$ ; **c)** at center of a collar,  $M=0.13$ ; **d)** midway between two collars,  $M=0.17$ .



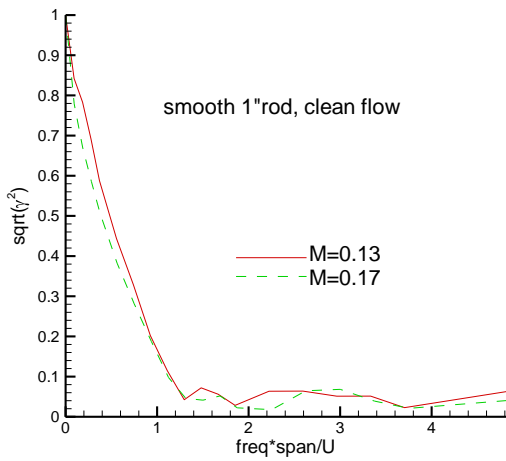
**Figure 27.** Configuration 21 (1" rod with wire wrap). Axial vorticity contours and in-plane velocity vectors. Smooth rod, clean flow. Measurements performed at model midspan **a)**  $M=0.13$ ; **b)**  $M=0.17$ .



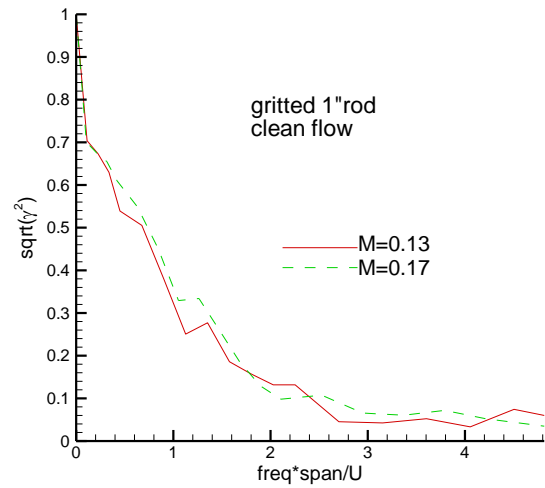
**Figure 28.** 1" rod. Cross spectral density between the stationary and traversing hot-wires. The two hot-wires are aligned along the span of the rod. The spacing between the two probes is  $\Delta y=0.25"$ .



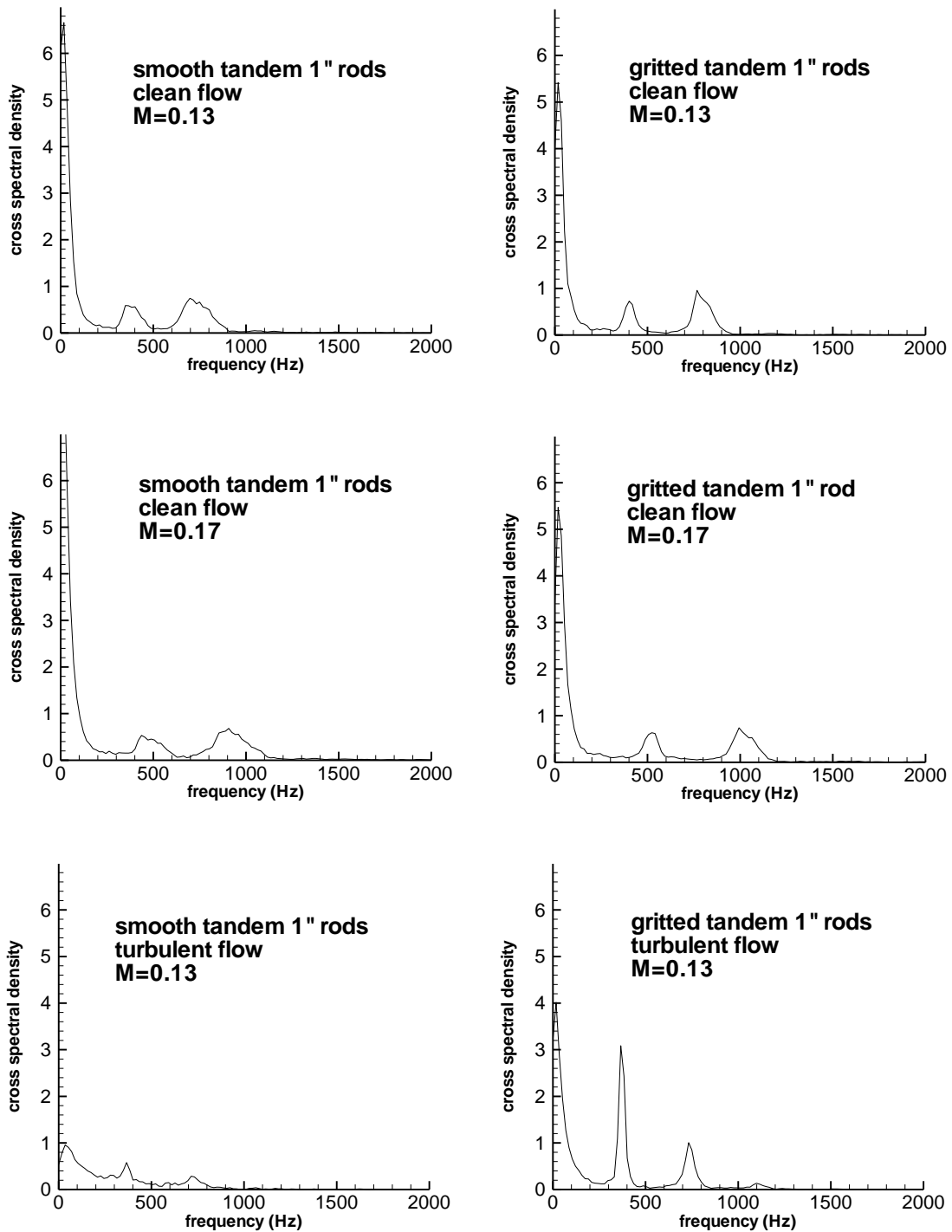
**Figure 29.** Spanwise coherence for a 1" rod.  $f = 2 f_0$ . The flow Mach number is 0.13.



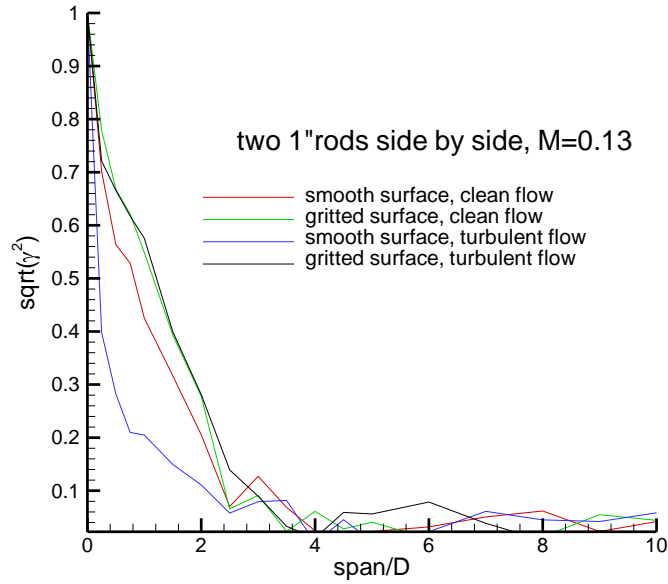
**Figure 30.** Spanwise coherence at  $f = 2 f_0$ . 1" rod, smooth surface, clean flow.



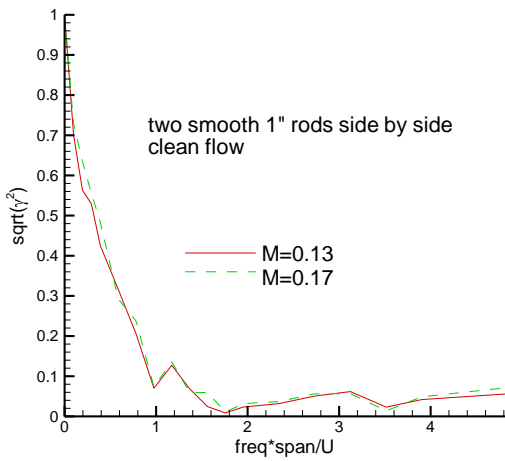
**Figure 31.** Spanwise coherence at  $f = 2 f_0$ . 1" rod, gritted surface, clean flow.



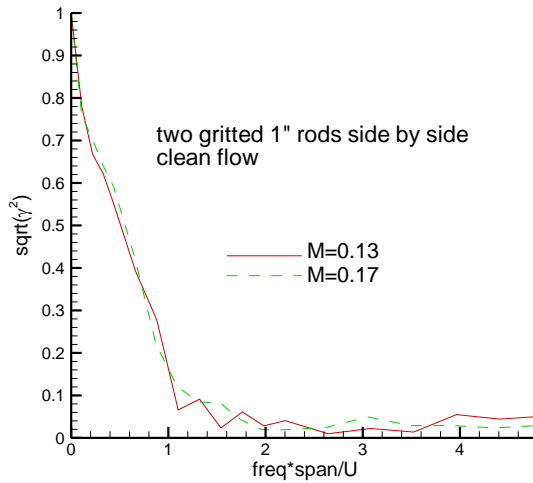
**Figure 32.** Two side by side 1" rods. Spacing center to center is 2". Cross spectral density between the stationary and traversing hot-wires. The two hot-wires are aligned along the span of one of the two rods. The spacing between the two probes is  $\Delta y=0.25"$ .



**Figure 33.** Spanwise coherence,  $f = 2 f_0$ . Two 1" rods side by sides, centers 2" apart. The flow Mach number is 0.13.



**Figure 34.** Spanwise coherence at  $f = 2 f_0$ . Two 1" rods side by sides, centers 2" apart. Smooth surface, clean flow.



**Figure 35.** Spanwise coherence at  $f = 2 f_0$ . Two 1" rods side by sides, centers 2" apart. Gritted surface, clean flow.

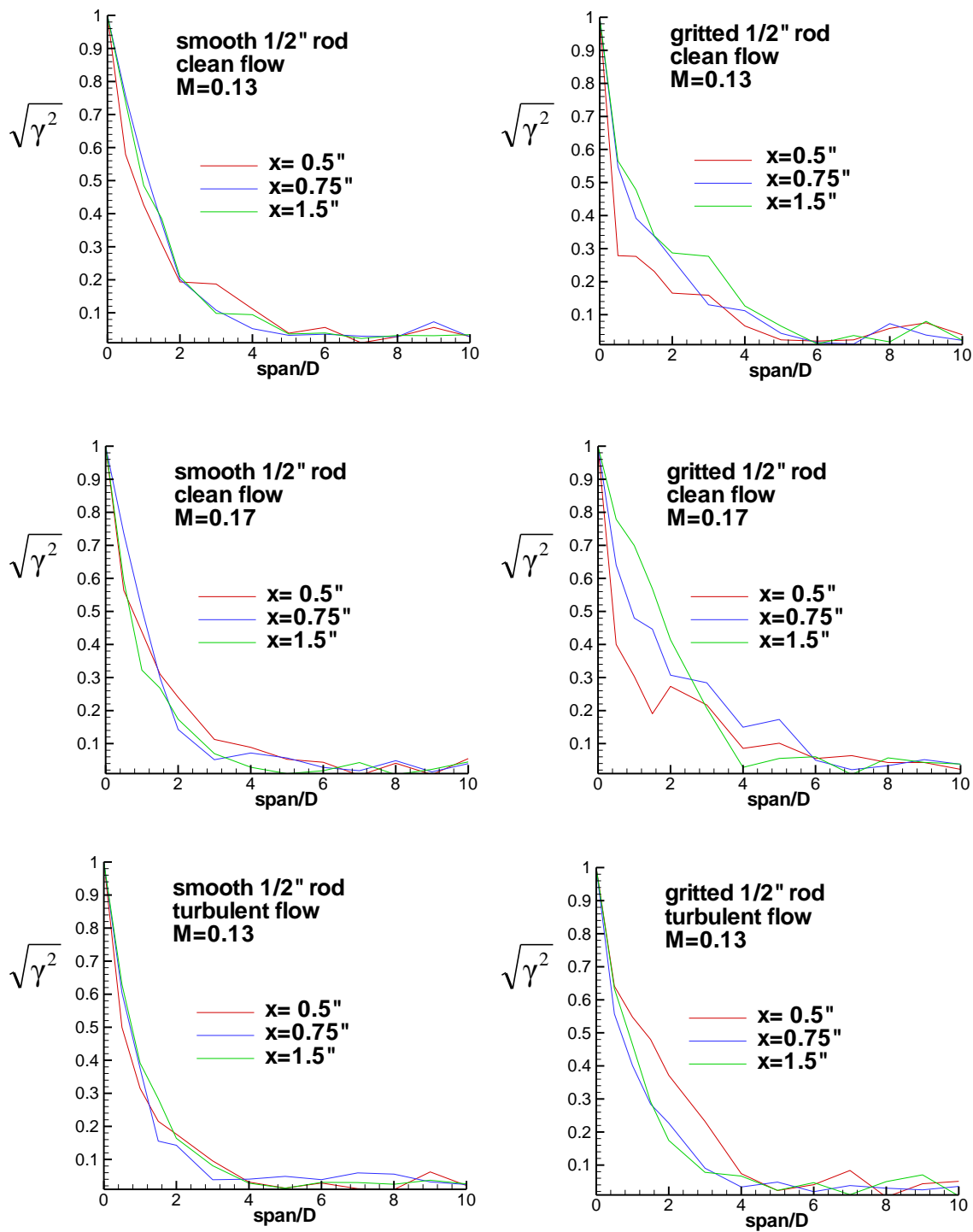
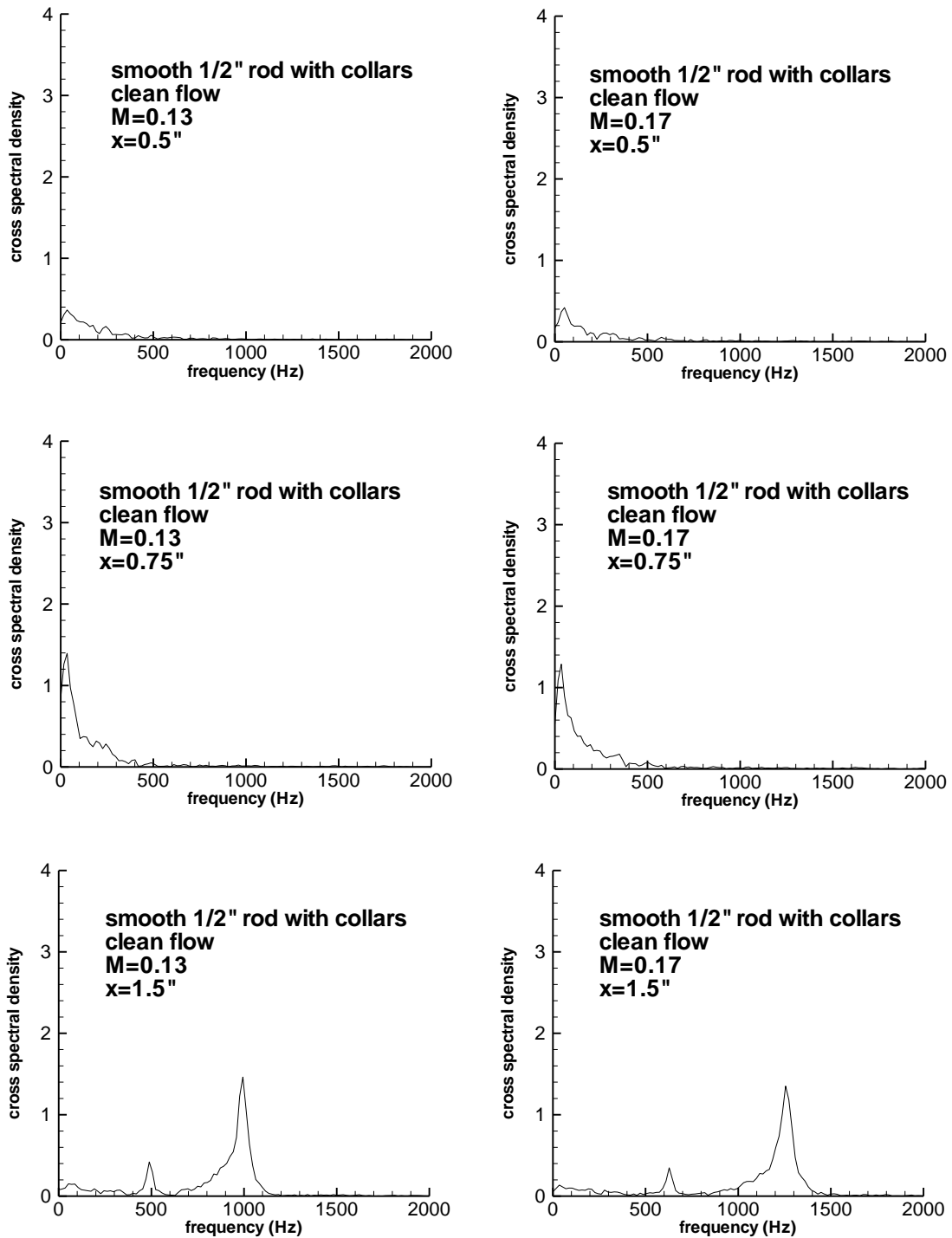
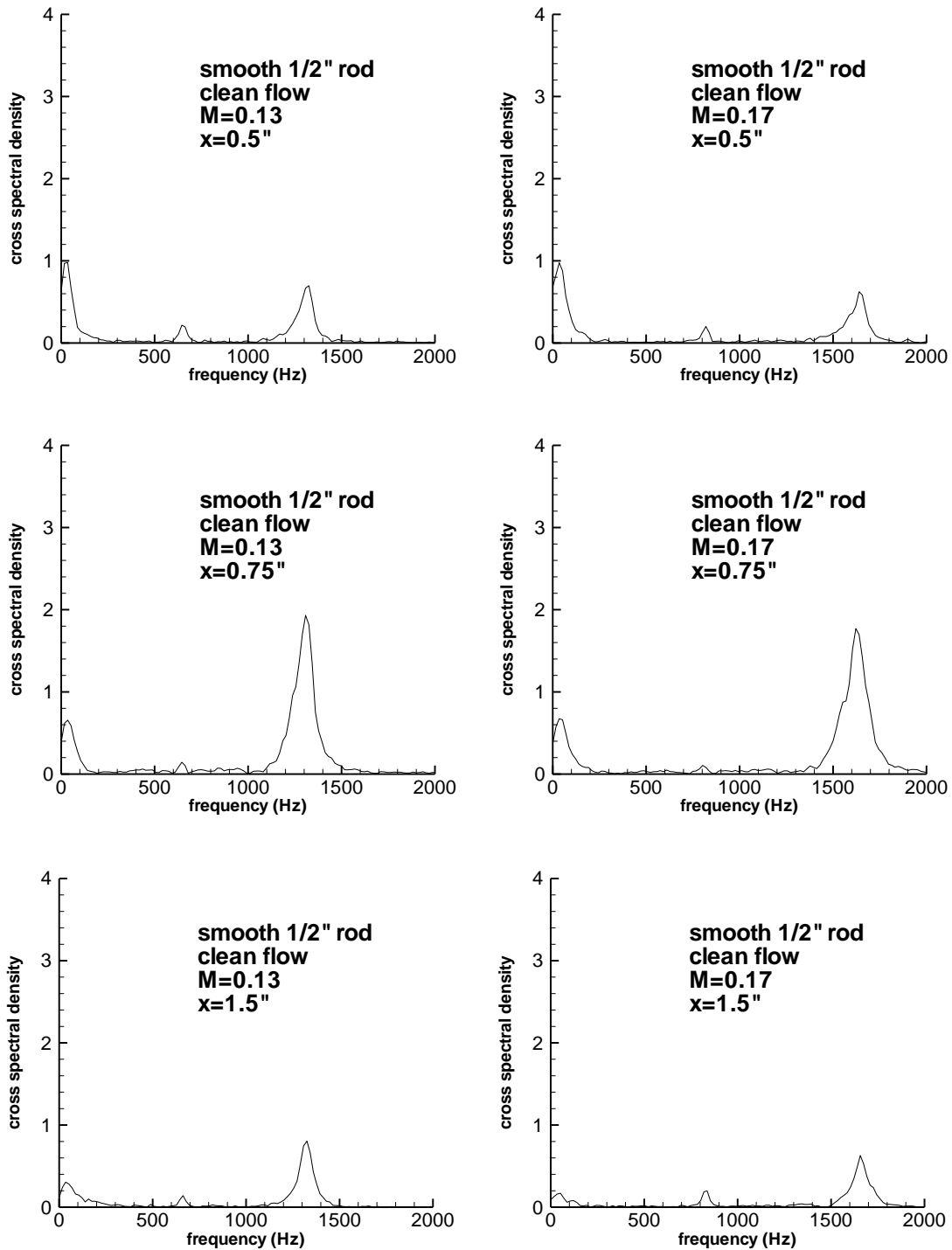


Figure 36. Spanwise coherence for a 1/2" rod.  $f = 2 f_0$ .

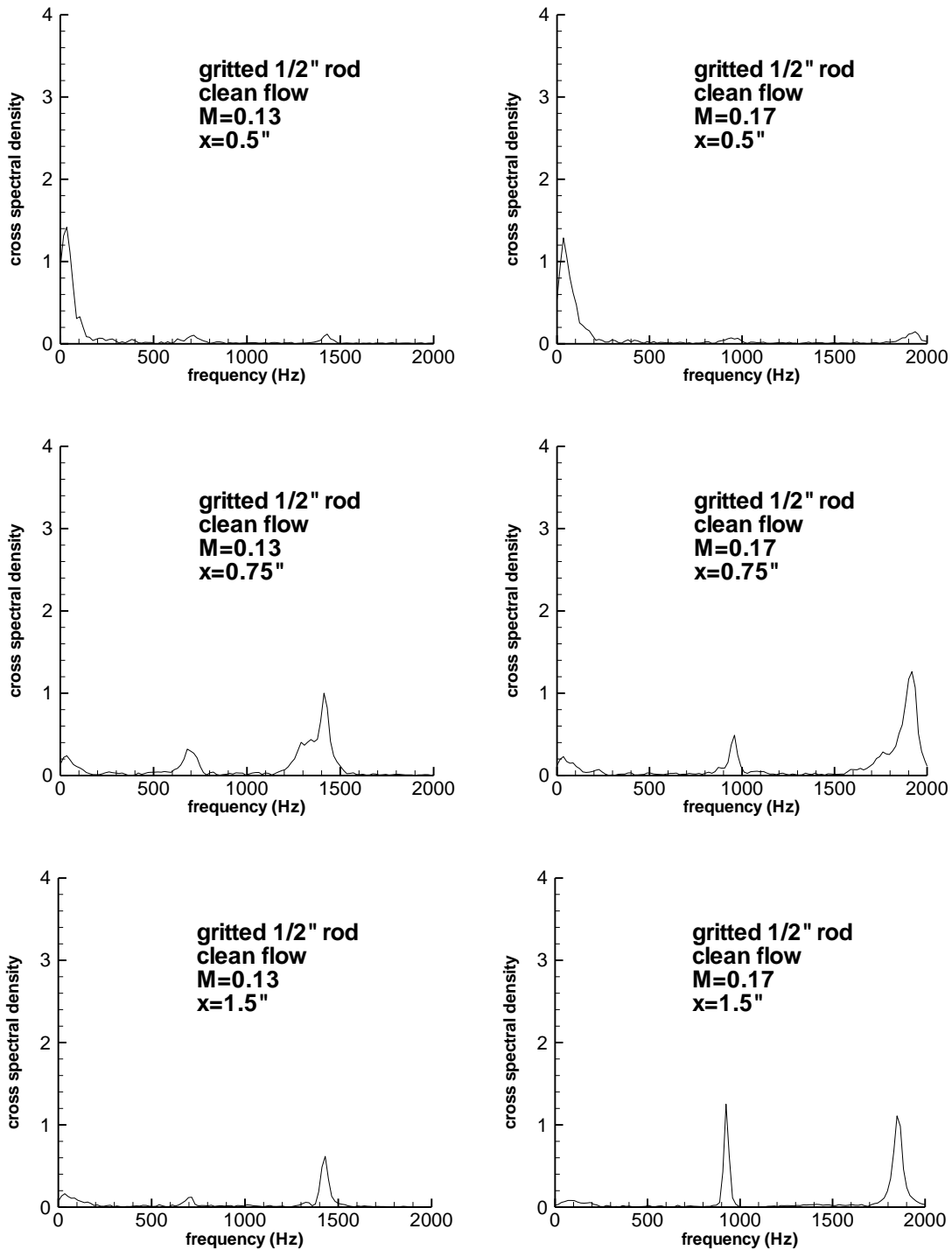




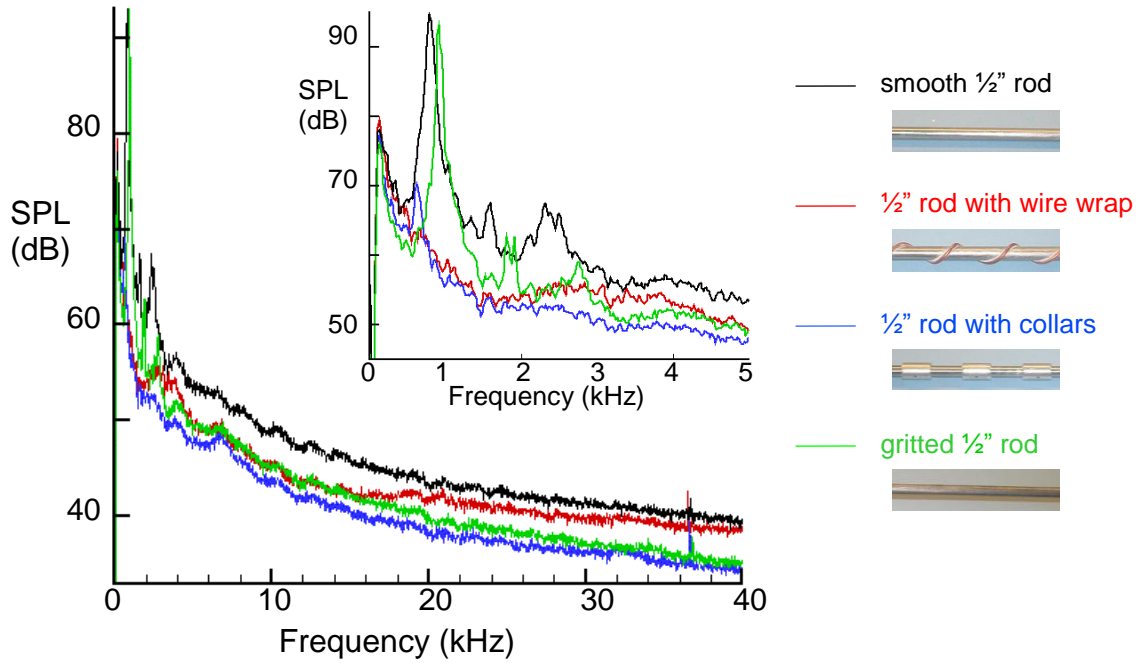
**Figure 37.** 1/2" rod with collars. Cross spectral density between the stationary and traversing hot-wires. The two hot-wires are aligned along the span of the rod. The spacing between the two probes is  $\Delta y=0.25"$ .



**Figure 38.** Smooth 1/2" rod. Cross spectral density between the stationary and traversing hot-wires. The two hot-wires are aligned along the span of the rod. The spacing between the two probes is  $\Delta y=0.25"$ .



**Figure 39.** Gritted 1/2" rod. Cross spectral density between the stationary and traversing hot-wires. The two hot-wires are aligned along the span of the rod. The spacing between the two probes is  $\Delta y=0.25"$ .



**Figure 40.** Noise spectra for the 1/2" rod. Four configurations: smooth or gritted 1/2" rod, smooth 1/2" rod with collars or with wire wrap. Clean incoming flow. Mach number 0.17.

**REPORT DOCUMENTATION PAGE**

*Form Approved  
OMB No. 0704-0188*

The public reporting burden for this collection of information is estimated to average 1 hour per response, including the time for reviewing instructions, searching existing data sources, gathering and maintaining the data needed, and completing and reviewing the collection of information. Send comments regarding this burden estimate or any other aspect of this collection of information, including suggestions for reducing this burden, to Department of Defense, Washington Headquarters Services, Directorate for Information Operations and Reports (0704-0188), 1215 Jefferson Davis Highway, Suite 1204, Arlington, VA 22202-4302. Respondents should be aware that notwithstanding any other provision of law, no person shall be subject to any penalty for failing to comply with a collection of information if it does not display a currently valid OMB control number.  
**PLEASE DO NOT RETURN YOUR FORM TO THE ABOVE ADDRESS.**

<b>1. REPORT DATE (DD-MM-YYYY)</b> 01-03-2010		<b>2. REPORT TYPE</b> Technical Memorandum		<b>3. DATES COVERED (From - To)</b>	
<b>4. TITLE AND SUBTITLE</b> Landing Gear Components Noise Study - PIV and Hot-Wire Measurements				<b>5a. CONTRACT NUMBER</b>	
				<b>5b. GRANT NUMBER</b>	
				<b>5c. PROGRAM ELEMENT NUMBER</b>	
<b>6. AUTHOR(S)</b> Hutcheson, Florence V.; Burley, Casey L.; Stead, Daniel J.; Becker, Lawrence E.; Price, Jennifer L.				<b>5d. PROJECT NUMBER</b>	
				<b>5e. TASK NUMBER</b>	
				<b>5f. WORK UNIT NUMBER</b> 561581.02.08.07	
<b>7. PERFORMING ORGANIZATION NAME(S) AND ADDRESS(ES)</b> NASA Langley Research Center Hampton, VA 23681-2199				<b>8. PERFORMING ORGANIZATION REPORT NUMBER</b>  L-19839	
<b>9. SPONSORING/MONITORING AGENCY NAME(S) AND ADDRESS(ES)</b> National Aeronautics and Space Administration Washington, DC 20546-0001				<b>10. SPONSOR/MONITOR'S ACRONYM(S)</b>  NASA	
				<b>11. SPONSOR/MONITOR'S REPORT NUMBER(S)</b>  NASA/TM-2010-216209	
<b>12. DISTRIBUTION/AVAILABILITY STATEMENT</b> Unclassified - Unlimited Subject Category 71 Availability: NASA CASI (443) 757-5802					
<b>13. SUPPLEMENTARY NOTES</b>					
<b>14. ABSTRACT</b> PIV and hot-wire measurements of the wake flow from rods and bars are presented. The test models include rods of different diameters and cross sections and a rod juxtaposed to a plate. The latter is representative of the latch door that is attached to an aircraft landing gear when the gear is deployed, while the single and multiple rod configurations tested are representative of some of the various struts and cables configuration present on an aircraft landing gear. The test set up is described and the flow measurements are presented. The effect of model surface treatment and freestream turbulence on the spanwise coherence of the vortex shedding is studied for several rod and bar configurations.					
<b>15. SUBJECT TERMS</b> Noise; Flow measurements; Landing gear; Rod and bar configurations; Wake flow					
<b>16. SECURITY CLASSIFICATION OF:</b>			<b>17. LIMITATION OF ABSTRACT</b>	<b>18. NUMBER OF PAGES</b>	<b>19a. NAME OF RESPONSIBLE PERSON</b>
<b>a. REPORT</b>	<b>b. ABSTRACT</b>	<b>c. THIS PAGE</b>			STI Help Desk (email: help@sti.nasa.gov)
U	U	U	UU	53	<b>19b. TELEPHONE NUMBER (Include area code)</b> (443) 757-5802